Potential impact of shipping to air pollution in the Mediterranean region – a multimodel evaluation: Comparison of photooxidants NO_2 and O_3

Lea Fink[1], Matthias Karl[1], Volker Matthias[1], Sonia Oppo[2], Richard Kranenburg[3], Jeroen Kuenen[3], Jana Moldanova[4], Sara Jutterström[4], Jukka-Pekka Jalkanen[5], Elisa Majamäki[5]

[1]Helmholtz-Centre Hereon, Institute of Coastal Environmental Chemistry, 21502 Geesthacht, Germany
[2]AtmoSud, Air Quality Observatory in the Provence-Alpes-Côte d'Azur region, 13006 Marseille, France
[3]TNO, Netherlands Organization for Applied Scientific Research, 3584 CB Utrecht, The Netherlands
[4]IVL, Swedish Environmental Research Institute, 411 33 Göteborg, Sweden
[5]FMI, Finnish Meteorological Institute, FI-00560 Helsinki, Finland

Correspondence to: Lea Fink (lea.fink@hereon.de)

Abstract. Shipping has a significant share to the emissions of air pollutants such as NO_x and particulate matter (PM), and the global maritime transport volumes are projected to increase further in the future. The Mediterranean Sea contains the major route for short sea shipping within Europe and contains the main shipping route between Europe and East Asia. Thus, it is a highly frequented shipping area, and high levels of air pollutants with significant potential impacts from shipping emissions are observed at monitoring stations in many cities along the Mediterranean coast.

The present study is part of the EU H2020 project SCIPPER (Shipping contribution to Inland Pollution Push for the Enforcement of Regulations). Five different regional chemistry transport models (CAMx, CHIMERE, CMAQ, EMEP, LOTOS-EUROS) were used to simulate the transport, chemical transformation and fate of atmospheric pollutants in the Mediterranean Sea for 2015. Shipping emissions were calculated with STEAM version 3.3.0, and land-based emissions were taken from the CAMS-REG v2.2.1 dataset for a domain covering the Mediterranean Sea on a resolution of 12x12 km² (or 0.1° x 0.1°). All models used their standard setup for further input. Potential impact of ships was calculated with the zero-out method. The model results were compared against each other and measured background data at monitoring stations.

The model results are differing regarding the time series and pattern but are similar results concerning the overall underestimation of NO_2 and overestimation of O_3. The potential impact from ships to the total NO_2 concentration was especially high at the main shipping routes and coastal regions (25% to 85%). The potential impact from ships to the total O_3 concentration was lowest in regions with the highest NO_2 impact (down to -20%). CAMx and CHIMERE simulated the highest potential impacts of ships to the NO_2 and O_3 air concentrations. Additionally, the strongest correlation was found between CAMx and CHIMERE, which can be traced back to the usage of the same meteorological input data. The other models used different meteorological input due to their standard setup. The CMAQ, EMEP and LOTOS-EUROS simulated values were within one range for the NO_2 and O_3 air concentrations. Regarding simulated deposition, larger differences between the models were found when compared to air concentration. These uncertainties and deviations between models are

caused by deposition mechanisms, which are unique within each model. A reliable output from models simulating ships potential impacts can be expected for air concentrations of NO_2 and O_3.

1 Introduction

Shipping activity and freight transport via ships are growing, and previous studies have shown that the relative potential impact from shipping to total air pollution will also increase (Brandt et al., 2013). Once in the atmosphere, these emissions are transported over several hundreds of kilometers, with 70 % of shipping emissions occurring less than 400 km from the coast (Eyring et al., 2010; Endresen et al., 2003). Several previous studies have pointed out the negative effect of shipping emissions on the concentration of air pollutants, playing a role as greenhouse gases, impacting human health or contributing to acidification and eutrophication (Tysro and Berge, 1997; Corbett and Fischbeck, 1997; Corbett et al., 1999). An overview over the current knowledge of effects of shipping on air quality and the human health worldwide is given in a review by Contini et al. (2021).Nevertheless, maritime transport plays a vital role in the international trade of goods worldwide as well as in the European Union (EU). The Eurostat Press Office (2016) stated that for 2015, the value of EU trade of goods with non-EU countries transported by the sea was approximately 51% of EU traded goods. The Mediterranean Sea contains one main shipping route between Europe and Asia, being the region in Europe with maximal impact from shipping emissions to gaseous pollutants, in addition to the North Sea (Viana et al., 2014).

Additionally, as one of the fastest growing sources of greenhouse gas emissions, shipping emissions directly result in health problems and have adverse effects on ecosystems (Brandt et al., 2013). The wide range of gaseous pollutants, such as nitrogen oxides (NO_x = NO_2 + NO), coming from shipping emissions have negative impacts by forming smog and acid rain and contribute to eutrophication (Jägerbrand et al., 2019; Brandt et al., 2013; Karl et al., 2019b; Matthias et al., 2010).
Moreover, NO_x, as a primary pollutant, plays an important role in the formation of O_3 and in the deposition of reactive nitrogen compounds (Eyring et al., 2010). The oxidation of VOCs (volatile organic compounds) produces ozone in the troposphere when NO_x and sunlight are present. O_3 can inflame and damage the respiratory system, make the lungs more susceptible to infection and intensify lung diseases (EPA, 2021). Although it is not directly emitted, O_3 is an important compound in photochemistry. Especially in the Mediterranean Sea during summer, when radiation is high, the contribution of shipping emissions to mean surface O_3 concentrations can be significant (Aksoyoglu et al., 2016).
Atmospheric nitrogen deposition mainly comes from agricultural activities and combustion processes such as those in shipping (Aksoyoglu et al., 2016). This increase in bioavailable nitrogen deposition causes eutrophication (Jägerbrand et al., 2019). The deposition of O_3 affects the plant's stomata, damages the plants, changes water and carbon cycling and reduces crop yields (Clifton et al., 2020).

Chemistry transport models (CTMs) can be applied to simulate the transport of air pollutants as well as chemical transformation and deposition. These models can be used at different scales, depending on the domain they cover and the question to be answered.

Although shipping emissions have a significant impact on air pollution by NO_2 in the Mediterranean Sea (Marmer and Langmann, 2005), few regional-scale chemistry transport modeling studies have focused on this domain. A literature review study focusing on the assessment of the impacts of shipping emissions on air quality in European coastal areas by Viana et al. (2014) showed that studies regarding shipping emissions in the Mediterranean Sea emphasize PM_x levels and their chemical composition instead of gaseous pollutants. Marmer and Langmann (2005) investigated the Mediterranean Sea, but on a larger scale or without the comparison of different CTMs. Other studies focus on smaller domains over the Iberian Peninsula (Baldasano et al., 2011; Nunes et al., 2020), the eastern part of the Mediterranean Sea with the Arabian Peninsula (Večeřa et al., 2008; Tadic et al., 2020; Celik et al; Friedrich et al., 2021) or urban scale and harbor cities (Schembari et al., 2012; Donateo et al., 2014; Prati et al., 2015). However, none of these studies modeled the potential impact of ships on a regional scale with a subsequent model comparison of different CTMs. A comparison of results of regional-scale chemistry transport models was performed for the Baltic Sea or for all of Europe (Karl et al., 2019a; Im et al., 2015a) but not exclusively for the western Mediterranean region.

Dry deposition is a substantial sink for atmospheric pollutants. Furthermore, it determines the net flux of pollutants to the Earth's surface (Galmarini et al., 2021). Accurate estimates of dry deposition are required for reliable predictions of atmospheric concentrations, since it is an important loss process scaling with concentrations close to the ground (Emerson et al., 2020; Vivanco et al., 2018). NO_2 deposition contributes to eutrophication, followed by biodiversity loss, whereas O_3 dry deposition injures plant tissues and reduces plant productivity (Vivanco et al., 2018; Clifton et al., 2020). The deposition of N and S was investigated in previous studies (i.e., Vivanco et al., 2018; Jutterström et al., 2021; Galmarini et al., 2021). Nevertheless, few studies have performed model intercomparison for dry deposition; thus far, none of the studies have focused on ship impact over the western part of the Mediterranean Sea. Comparing the dry deposition mechanisms of different models is essential since these mechanisms are unique for each model. In Galmarini et al. (2021), deposition schemes of different models were compared, including LOTOS-EUROS and CMAQ, which are also part of the present study. They showed, i.e., differences in surface resistance calculation and deposition pathways: LOTOS-EUROS uses a single deposition pathway to soil. In comparison, CMAQ uses two deposition pathways for deposition to soil (one for vegetation-covered and one for bare soil).

Additionally, another important factor is the land use-land cover (LUCL) on which dry deposition strongly depends but is unique in each model. This was also stated by Vivano et al. (2018), explaining that even if models apply similar algorithms in their deposition schemes, they may use different land use or leaf index area data. Thus, mainly over land areas, differences in model simulations are to be expected. A similar mechanism and model results for dry deposition is expected over water and therefore over most of the considered domain in the present study.

The Ship Traffic Emission Assessment Model (STEAM) has been previously applied to evaluate shipping emissions in different regions, such as the North Sea or Baltic Sea (Jalkanen et al., 2009; Jonson et al., 2015; Aulinger et al., 2016; Barregard et al., 2019) or the Iberian Peninsula (Nunes et al., 2020), as well as in European (Jalkanen et al., 2016) and global regions (Johansson et al., 2017). However, the model has not been previously used in a study focusing entirely on the western Mediterranean Sea region.

In addition, the Mediterranean Sea is not yet the ECA (Emission Control Area). The contracting parties of the Barcelona Convention agreed to designate the Mediterranean Sea as an Emission Control Area for Sulfur emissions (MedECA) by 2025. Nevertheless, although SO_2 emissions must be reduced by 50 % to 80 % by 2030, NO_x emissions from ships will grow without further control and likely exceed emissions from land-based sources in the European Union after 2030 (Cofala et al., 2018). Furthermore, the current state of air pollution is calculated to have a basis for investigating the effects of additional legislation. It is important to simulate the potential impact of ships to several air pollutants to show the impact of ships in a larger area.

The Horizon 2020 SCIPPER project (Shipping Contributions to Inland Pollution Push for the Enforcement of Regulations) aims to determine how existing regulations ensure compliance with the legislation on emissions to air from ships. One part of this project was to focus on CTMs and their possible supportive effects in the monitoring of compliance of threshold levels.

The present study compares and evaluates five different CTMs concerning their predictions of the dispersion and transformation of air pollutants. The main focus of this study is to compare the results of model simulations regarding the potential ship impact to atmospheric concentrations and dry deposition of NO_2 and O_3. Using this comparison, important differences in the photochemical processing between the CTMs and the balance of photochemistry in the models focusing on shipping will be highlighted. Furthermore, the model performance was quantified by comparing the simulated data against the measured data of air pollutants at background stations in coastal areas of the Mediterranean Sea. The performance of the models was compared based on statistical indicators.

By using five different CTMs in this part of the SCIPPER project, a more robust estimate of the potential ship impact to the air pollution can be given. To date, the present study is the first multimodel study to compare potential ship impacts to five regional-scale CTMs in the Mediterranean Sea.

2 Materials and Methods

2.1 Models

Five different regional-scale CTMs were used for this study, run by four institutions: CAMx and CHIMERE by AtmoSud, CMAQ by Helmoltz Centre Hereon, EMEP by IVL Swedish Environmental Research Institute and LOTOS-EUROS by TNO Netherlands Organization for applied scientific research.

The goal was to have a model setup as similar as possible for all models to receive comparable simulations. As a base, an inner and outer domain with grid resolution was established. Additionally, the emissions were provided for one year. Especially of importance in the present study was the method for calculating the potential ship impact.

An overview of the input data is shown in Table 1. Input data were the same for shipping emissions using STEAM (version 3.3.0.; Jalkanen et al., 2009; Jalkanen et al., 2012; Johansson et al., 2013; Johansson et al., 2017), land-based emissions (CAMS-REG, v2.0) as well as projection (WGS84_lonlat), domain (Mediterranean Sea), resolution (0.1° x 0.1°, 12 x 12 km) and the modeled year (2015). Input data were different for meteorological input data, boundary and initial conditions because the CTMs used their standard setup.

The model simulation runs should all contain NO_2 and O_3 in µg/m³ at an hourly resolution on a 2D grid from the lowest layer and be provided as a netcdf file following CF conventions. The lowest layer on the ground was used in the present study.

With all CTMs, a reference run for the current air quality situation was performed, including all emissions (base case). Furthermore, all models did one run without the emissions from shipping (noship case). The difference between the calculations with all emissions and the calculation without shipping emissions is used to determine the potential impacts of ships to the ambient pollutant concentration. This method shows the change of an emission reduction and the maximal effect, by having a complete switch-off from shipping activity in the noship run. Thus, it is referred to as zero-out method. This was done for all five models.

Table 1: Main model parameters and input data for the five chemical transport models.

Model parameter	CAMx	CHIMERE	CMAQ	EMEP	LOTOS-EUROS
Grid resolution inner domain	12x12 km²	12x12 km²	12x12 km²	0.1°x 0.1°	0.1°x 0.1°
Grid resolution outer domain	36x36 km²	36x36 km²	36x36 km²	none	0.5°x 0.25°
Land-based emissions	CAMS-REG	CAMS-REG	CAMS-REG	CAMS-REG	CAMS-REG
Shipping emissions	STEAM	STEAM	STEAM	STEAM	STEAM
Biogenic emissions	MEGAN Model v2.03	MEGAN Model v2.04	MEGAN Model v3	Calculated online	Calculated online
Sea salt emissions	PSAT and OSAT modules	Calculation based on Monahan et al. (1986)	Calculation based on Kelly et al. (2010)	Calculation based on Monahan et al. (1986) and Mårtensson et al. (2003)	Calculation based on Monahan et al. (1986) and Mårtensson et al. (2003)
Dust emissions	Based on approach used in global EMAC (ECHAM/ MESSy; Klingmueller et al.,	Calculated online	Not considered	Key parameter is wind friction velocity	Calculated online

	2017; Astitha et al., 2012).				
Meteorological driver	WPS/WRF	WPS/WRF	COSMO-5 CLM	ECMWF (IFS)	ECWMF (IFS)
Boundary conditions	Mozart-4 output	Gaseaous species: LMDz-INCA model Aerosols: GOCART model	IFS_CAMS cycle45r1	Boundary conditions provided with the open source modeldistribution for year 2015	CAMS C-IFS
Chemical mechanism	CB05	MELCHIOR2	CB05	EmChem 19a	CBM-IV
Dry deposition scheme	Resistance model of Zhang et al. (2003)	Dry deposition is as in Wesely (1989)	Dry deposition scheme M3Dry (Pleim, 2001)	As described in Simpson et al. (2012)	Resistance approach following Erisman et al. (1994)

2.1.1 Model description CAMx

CAMx (Comprehensive Air Quality Model with Extensions) is a Eulerian photochemical dispersion model developed by Ramboll Environ. Version CAMx v6.50 of the model was used in the present study.

For this study, a first domain with a 36 km resolution was defined at the European scale. A second nested domain was defined, named MEDI12 (147x249 points), and covered the center of Europe with a resolution of 12 km. Both meteorological and chemical transport simulations were provided for these domains. WRFv3.9 was run for the simulation of meteorological conditions with 28 vertical layers up to 50 hPa, with FNL data for initial conditions.

For the CAMx simulation, boundary conditions from the Mozart-4 was used.

Sea salt emissions are calculated in the SEASALT pre-processor of CAMx. This program generates aerosol emissions of sodium, sulfate and chloride, and gaseous emissions of chlorine using CAMx-ready meteorological and landuse files. The sea salt emissions program calculates the flux of sea salt over the open ocean using parameterizations developed by Ovadnevaite et al. (2014). The surf zone aerosol flux is calculated by using Gong (2003) open ocean approach with an assumed 100% whitecap coverage. Biogenic emissions were calculated separately with the MEGANv2.03 (Model of Emissions of Gases and Aerosols from Nature; Guenther et al., 2006) and then included in the land-based emissions. WBDUST pre-processors delivers dust emissions in CAMx and generates gridded windblown dust emissions. The scheme is based on an updated approach used in the global EMAC (ECHAM/MESSy) atmospheric chemistry-climate model (Klingmueller et al., 2017; Astitha et al., 2012). The mechanism for lightning NO_x was not activated in CAMx.

The gas phase chemical mechanism is CB05, in which the NMVOC emissions are split into 13 species (TERP, ISOP, XYL, TOL, ETOH, MEOH, IOLE, OLE, ETH, ALD2, PAR, ETHA and FORM) and describe approximately 156 reactions. For

semivolatile inorganic species (sulfate, nitrate, and ammonium), the equilibrium concentration is calculated using the thermodynamic model ISORROPIA (Nenes et al., 1998). Fourteen vertical levels are simulated with a first layer height of approximately 10 km.

2.1.2 Model description CHIMERE

CHIMERE is an offline chemistry transport model developed by LMD-IPSL/CNRS (Menut et al., 2013). The CHIMERE2017r4 version of the model was used in this study.

WRFv3.9 (Weather Research and Forecasting Model) was run for the simulation of meteorological conditions with 28 vertical layers up to 5 0 hPa, with FNL data for initial conditions.

Concerning CHIMERE simulation, boundary conditions are monthly mean climatologies taken from the LMDz-INCA model (Laboratoire de Météorologie Dynamique General Circulation Model – INteraction with Chemistry and Aerosols; Schultz et al., 2006) for gaseous species and from the GOCART model (Global zone Chemistry Aerosol Radiation and Transport; Ginoux et al., 2001) for aerosols (desert dust, carbonaceous species and sulfate). Sea salt emissions were calculated as described in Monahan (1986). MEGAN Model v2.04 calculated biogenic emissions (Guenther et al., 2006). MEGAN is running directly by CHIMERE code and biogenic emissions are just generated before the air quality run. The mineral dust emissions are calculated on-line. The soil is represented by relative percentages of sand, silt and clay with the USGS soil texture (www.usgs.gov). The aeolian roughness length used in CHIMERE is the GARLAP (Global Aeolian Roughness Lengths from ASCAT and PARASOL) dataset as in Prigent et al. (2012). There is no treatment of NO_x lightning in CHIMERE.

The gas phase chemical mechanism is MELCHIOR2 (Modele Lagrangien de Chimie de l'Ozone a l'echelle Regionale), in which the NMVOC emissions are split into 10 species (C2H6, NC4H10, C2H4, C3H6, C5H8, OXYL, HCHO, CH3CHO, CH3COE and APINEN) and describe approximately 120 reactions. For semivolatile inorganic species (sulfate, nitrate, and ammonium), the equilibrium concentration is calculated using the thermodynamic model ISORROPIA (Nenes et al., 1998). Nine vertical levels are selected with a first layer height at 20 m to 25 m.

2.1.3 Model description CMAQ

The CMAQ Model v5.2 with the aero6 model calculates on the basis of emission input data air concentration as well as deposition fluxes of atmospheric gases and aerosols (Byun and Schere, 2006; Appel et al., 2017). Atmospheric chemistry is used by the chemical Carbon Bond 5 (CB05) mechanism (Yarwood et al., 2005) cb05tucl with updated toluene chemistry (Whitten et al., 2010), including the chlorine chemistry extension (CB05-TUCL; https://www.airqualitymodeling.org/index.php/CMAQv5.0_Chemistry_Notes, accessed May 2021). The aerosol scheme AERO6 is used for the formation of secondary inorganic aerosols. Sulfuric acid (H_2SO_4), nitric acid (HNO_3), hydrochloric acid (HCl) and ammonia (NH_3) gas phase – aerosol partition equilibrium is solved by the ISORROPIA mechanism (Fountoukis

and Nenes, 2007; Nenes et al., 1998). Contained within is the formation of secondary organic aerosol (SOA) from isoprene, terpenes, benzene, toluene, xylene and alkanes (Carlton et al., 2010; Pye and Pouliot, 2012).

Sea salt emissions were calculated as described in Kelly et al. (2010). Biogenic emissions (NMVOC from vegetation and soil NO) were calculated previously with the MEGAN Model v3 (Guenther et al., 2012) and then included into the land-based emissions. Emissions of windblown dust were not considered. CMAQ models 30 vertical layers, with the lowest layer from 0 m to 42 m and the second layer from 42 m to 85 m. The NO_x lightning treatment in CMAQ was not activated for the present study.

The COSMO model simulated the meteorological data for CMAQ, applying the version COSMO5-CLM16 (Schultze and Rockel, 2018; Petrik et al., 2021). The MCIP (Meteorology-Chemistry Interface Processor) processed meteorological model output into the input format required for CMAQ. The vertical resolution of the meteorological model was 40 terrain-following geometric height levels up to 22 km. The Boundary Condition driver used was IFS-CAMS cycle45r1 (Integrated Forecasting System – Copernicus Atmosphere Monitoring Service; Inness et al., 2019) with a vertical resolution of 60 sigma levels up to 65 km.

To prevent the effects from initial conditions on the simulated atmospheric concentrations in 2015, the model run started with a spin up run in mid-December 2014. The grid size of the Mediterranean Sea domain was 12 x 12 km², nested in a 36 x 36 km² domain covering all of Europe.

2.1.4 Model description EMEP

The EMEP MSC-W (European Monitoring and Evaluation Programme, Meteorological Synthesizing Centre – West, https://www.emep.int/mscw/index.html, assessed June 2021) model is a limited area, terrain-following hybrid coordinate model designed to calculate air concentrations and deposition fields for major acidifying and eutrophying pollutants, photooxidants and particulate matter (Simpson et al., 2012; Simpson et al., 2020).

In this study, a 0.1° x 0.1° resolution grid on long–lat projection and with 20 vertical levels was used. The meteorological input data are based on forecast experiment runs with the Integrated Forecast System (IFS), a global operational forecasting model from the European Centre for Medium-Range Weather Forecasts (ECMWF). The meteorological fields are retrieved on 0.1° x 0.1° long–lat coordinates. Vertically, the fields on 60 eta (η) levels from the IFS model are interpolated onto the 20 EMEP eta levels.

The model version used was rv4.34 with chemical mechanism EmChem 19a (Simpson et al., 2012; Simpson et al., 2020). The mechanism builds on surrogate VOC species (Simpson et al., 2012; extended with benzene and toluene) and has 171 gas phase and heterogeneous reactions. The model always assumes equilibrium between the gas and aerosol phases using the MARS equilibrium module (Model for an Aerosol Reacting System) of Binkowski and Shankar (1995). For secondary organic aerosol (SOA), a so-called volatility basis set (VBS) approach (Robinson et al., 2007; Donahue et al., 2009; Bergström et al., 2012) is used. All primary organic aerosol (POA) emissions are treated as nonvolatile to keep emission totals of both PM and VOC

components the same as in the official emission inventories, while the semivolatile ASOA and BSOA species are assumed to oxidize (age) in the atmosphere by OH reactions (Simpson et al., 2012).

The generation of sea salt aerosol over oceans is driven by the surface wind, and the EMEP model's parameterization scheme for calculating sea salt generation is based on two source functions, those of Monahan et al. (1986) and Mårtensson et al. (2003). The following natural emissions are calculated in the model for each grid cell and at every model time step: Biogenic emissions of isoprene and monoterpenes use near-surface air temperature and photosynthetically active radiation. Soil NO emissions from soils of seminatural ecosystems are specified as a function of N deposition and temperature. The key parameter driving dust emissions is wind friction velocity. Additionally, daily emissions from forest and vegetation fires are taken from the "Fire INventory from NCAR version 1.0" (FINNv1; Wiedinmyer et al., 2011). Emissions of NO_x from lightning are included as monthly averages of global 3-D fields on a T21 (5.65° ×5.65°) resolution (Köhler et al., 1995). For this study, the initial and boundary conditions provided with the open source model distribution for 2015 were used.

2.1.5 Model description LOTOS-EUROS

LOTOS-EUROS is a Eulerian chemistry transport model (Manders et al., 2017). The model simulates air pollution in the lower troposphere and is of intermediate complexity, allowing ensemble-based simulations and assimilation studies. LOTOS-EUROS performs hourly model output using ECMWF (European Centre for Medium-Range Weather Forecasts) meteorological data. The gas phase chemistry follows the TNO CBM-IV scheme (Schaap et al., 2008)..

For sea salt two parametrizations are used for online calculation of emissions, Mårtensson et al. (2003) for fine particles, and Monahan et al. (1986) for coarse particles. Biogenic emissions are calculated online during the CTM run. For isoprene, a tree species-dependent emission factor was used (Schaap et al., 2009; Beltman et al., 2013). NO emissions from soil were calculated as in Novak and Pierce (1993). Dust emissions are also calculated online for three sources of dust. Desert dust following Mokhtari et al. (2012) and road resuspension and dust from agricultural processes following a module developed by Schaap et al. (2009). There is no treatment of NO_x lightning in LOTOS-EUROS.

LOTOS-EUROS has a dynamical vertical layer structure with 5 layers in total. The first layer is at 25 m, while the second layer follows the meteorological boundary layer. On top of that, up to 3500 m and one top layer up to 5000 m above sea level two evenly distributed reservoir layers are defined. The model has participated in multiple model intercomparison studies (Bessagnet et al., 2016; Colette et al., 2017), showing overall good performance.

2.2 Model Domains and Nesting

The domain for the intercomparison of a section the Mediterranean Sea covered a spatial extent from longitude: -0.95° to 29.95° and latitude: 33.8° to 44.95°. The grid cell size used was 12 x 12 km² interpolated on a 0.1° x 0.1° grid nested in a larger 36 x 36 km² grid (except EMEP) covering all of Europe, as shown in Figure 1. Computational domains of the CTMs can be found in Supplement S1.

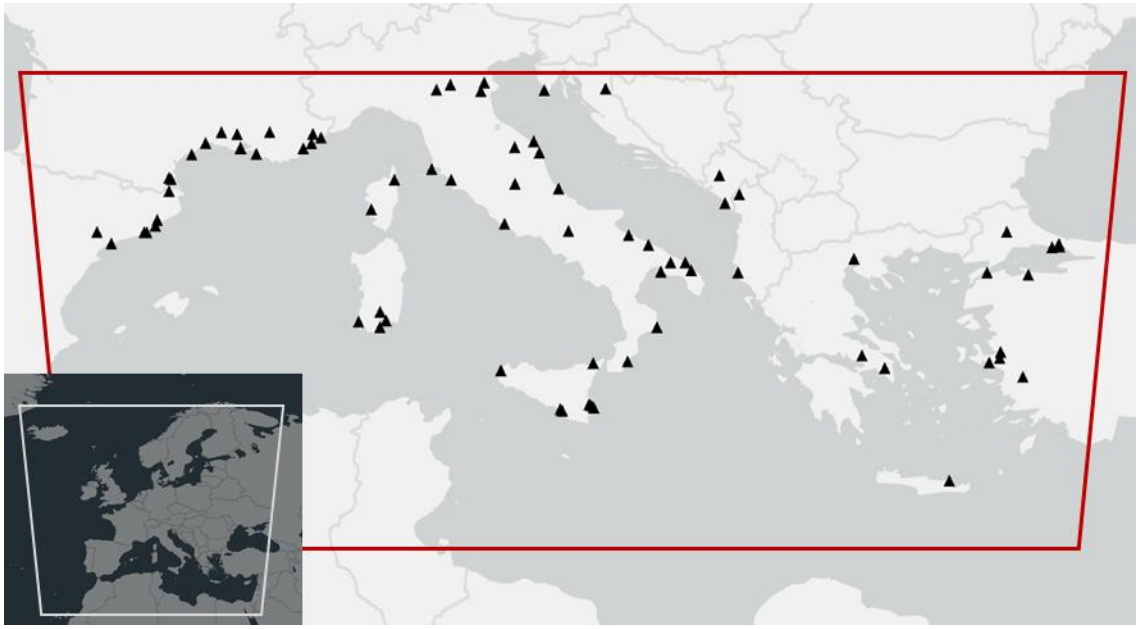

Figure 1: Domains and measurement stations. Red trapeze displays the 12 x 12 km² domain, black triangles are locations of measurement stations. On bottom left the larger 36 x 36 km² domain is displayed.

2.3 Emissions

2.3.1 Land-based Emissions

Annual anthropogenic land-based gridded emissions for 2015 obtained from the CAMS-REG v2.2 emission inventory were used as input by all five compared models. Gridded emission files contain GNFR (Gridded Nomenclature for Reporting) emission sectors for each country for the air pollutants NO_x, SO_2, NMVOC, NH_3, CO, PM_{10}, $PM_{2.5}$, and CH_4. The emissions are provided at a spatial resolution of 1/10° x 1/20° in longitude and latitude (i.e., ~ 6 x 6 km over central Europe).
The height distribution of emissions per GNFR sector was determined as described in Bieser et al. (2011b). The temporal distribution was determined by separating the annual emissions of each sector into hourly emission data with data splitting as described in Granier et al. (2019). PM was split as described in Bieser et al. (2011a), NO_x was split according to Manders-Groot et al. (2016). NMVOC emissions were given for different sectors, using the GNFR and were separated countrywise. This split was used as provided in the CAMS-REG v2.2 emission inventory (Granier et al., 2019). The species were afterwards split within each CTM according to their chemical mechanism.

2.3.1 Shipping Emissions

The shipping emission dataset produced with the STEAM model has a spatial resolution of 12 x 12 km² and a temporal resolution of 1 hour. The STEAM emissions are divided into two vertical layers (0 m to 36 m; 36 m to 1000 m) and are provided for mineral ash, carbon monoxide (CO), carbon dioxide (CO_2), elemental carbon (EC), NO_x, organic carbon (OC), $PM_{2.5}$, particle number count (PNC), sulfate (SO_4), SO_x (containing SO_2 and SO_3) and VOC. To reduce the number of generated emission maps and the computational resources needed to run the STEAM model, VOC emissions were divided into four categories based on how their emission factors change as a function of the engine load. Emissions of individual VOC species were calculated afterwards based on their mass fractions of the total emissions in the VOC group. Emission factors for VOC are based on the average values taken from various publications (Agrawal et al., 2008; Agrawal et al., 2010; Sippula et al., 2014; Reichle et al., 2015).

In CAMx, all shipping emissions are put in the first layer. For CHIMERE, all shipping emissions above 36 m and 88 % of the emissions below 36 m have been added to the second layer. Only 12 % of the emissions below 36 m were emitted in the first layer of the model. This was calculated based on the STEAM emission dataset and therein contained stack heights. Additionally, in CMAQ, shipping emissions were distributed in the two lowest layers, emissions below 36 m were attributed to the lowest layer, and emissions above 36 m were in the second layer. For EMEP simulations, the STEAM emissions were summed from hourly to daily emissions and attributed to the lowest layer (up to 90 m). In LOTOS-EUROS, emissions below 36 m are assigned ~ 70 % to the first layer, which is 25 m thick, and ~ 30 % to the second layer. Emissions above 36 m are divided over different height classes 30 % between 36 m and 90 m, 30 % between 90 m and 170 m, 30 % between 170 m to 310 m and 10 % between 310 cm and 470 m. Due to the dynamic second model layer (following the meteorological boundary layer), those emissions are put in the second and/or third model layer. In the case of a well-mixed and vertically extended

meteorological boundary layer (above 470 m), all emissions are in this second layer, whereas when the boundary layer is shallow, some emissions are put in the third layer.

2.4 Deposition Mechanisms

Deposition velocities for gaseous species in CHIMERE, CMAQ and LOTOS-EUROS are based on the formula introduced by Wesely (1989). This formula is the reciprocal sum of aerodynamic resistance (R_a), quasi-laminar sublayer resistance (R_b) and surface resistance (R_c). Nevertheless, all models differ in calculating the single variables. R_a depends on meteorology and surface roughness, which is model dependent. R_b is determined by the friction velocity, depending on the surface type. R_c is the bulk surface resistance, containing different components, i.e., leaf stomata, soil, leaf litter, etc. All of these components use input data that are unique for each model.

In CHIMERE, R_b is estimated following Hicks et al. (1987). The resistance R_c formulation follows Erisman et al. (1994) and the developments made in the EMEP model (Emberson et al., 2000; Simpson et al., 2003; Simpson et al., 2012). It uses a variety of additional resistances, mostly to account for stomatal and surface processes, both of which are depending on the land use type and season. In CMAQ, the m3dry mechanism was used, which takes R_a and R_b from the provided meteorological data. R_c is calculated in CMAQ as described in Pleim and Ran (2011).

In EMEP quasi-laminar layer resistance R_b is following Hicks et al. (1987). Surface resistance, R_c Surface (or canopy) resistance is the most complex variable in the deposition model of which the calculation is described in Simpson et al. (2012).The resistance R_b in LOTOS-EUROS is described following the EDACS system (Erisman et al., 1994). In van Zanten et al. (2010), the parametrizations of different resistances R_c that contribute to resistance for dry deposition of NO_2 and O_3 are described, depending on land use type. The Deposition of Acidifying Compounds (DEPAC) 3.11 module was used in LOTOS-EUROS, following the resistance approach (van Zanten et al., 2010; Wichink Kruit et al., 2012).

CAMx uses the gas resistance model of Zhang et al. (2003), which is very similar to the Wesely formulations with regard to R_a and R_b. However, the R_c is expressed as several more serial and parallel resistances, based on Wesely (1989) but with some adjustments within CAMx (Ramboll Environment and Health, 2020).

2.5 Observational Data/Statistical Analysis/Analysis of Model Results

Model results for total surface concentrations of NO_2 and O_3 from the five CTMs are evaluated against available measurements of the air quality monitoring network taken from the download service of Air quality of the European Environment Agency EEA (https://discomap.eea.europa.eu/map/fme/AirQualityExport.htm, 2021). NO_2 concentrations are monitored at 62 and O_3 at 48 background stations. Figure 1 shows the locations of the measurement stations, and detailed information on the stations is given in Appendix B.

The criteria for the selection of the stations were i) station type is “background”, ii) elevation is below 1000 m and iii) data for more than one of the pollutants NO_2, O_3 or $PM_{2.5}$ are available. The latter was chosen for further comparison in this intercomparison project. Preferably, stations close to the sea were chosen since simulating potential ship impacts were the

major focus of this study. There was no exact threshold of distance to the coastline assumed, but preferably stations at a distance < 30 km from the coast. Some stations further inland were chosen to check the model performance. Furthermore, the domain was divided into four parts ("west", "north", "south", "east"), and a roughly equal number of stations should be in each parcel (map in Supplements Figure S2). The measured concentrations at the stations were compared against the results of simulations of the CTMs. For this purpose, the grid cell of the respective monitoring station was determined, and modeled concentrations were taken from there.

To quantify the CTMs performance, the root mean square error of the modeled values (RMSE), normalized mean bias (NMB) and Spearman's correlation coefficient (R) were calculated for each monitoring station, as described in Appendix A. A categorization for correlation was performed as described in Schober et al. (2018), adjusted and displayed in Table 2.

Table 2: Interpretation of the correlation coefficient, as described in Schober et al (2018), adjusted.

Magnitude of Correlation Coefficient	Interpretation
0.00–0.39	Weak correlation
0.40–0.69	Moderate correlation
0.70–1.00	Strong correlation

Time series were used to compare the modeled daily mean concentrations to observations at exemplary stations. In addition, the annual mean ship impact was calculated based on hourly data. For a graphical comparison of the model performances R, NMB and RMSE, boxplots were used based on annual values calculated from hourly data at each station. For the intercomparison spatial distribution, annual mean values based on the hourly data are used. The correlation R between models was calculated for each grid cell based on hourly data.

3 Results and Discussion

In the following section, the results for NO_2 and O_3 model performance and spatial distribution will be shown. Afterward, O_x and NO_x will be displayed for a more detailed investigation of the photochemistry and lifetime of the species. The results of dry deposition of NO_2 and O_3 will be considered in Sect. 3.4.

3.1 Model Performance and Intercomparison

To evaluate the performance of the CTMs, simulated concentrations considering all emission sectors (base case) for annual values of 2015 were compared against actual measured data of NO_2 and O_3. Based on the results of the five models for the cases with (base case) and without shipping emissions (noship case), potential impacts of the shipping sector to the NO_2 and O_3 concentrations were estimated. Figures of spatial distribution display the annual mean values for 2015 and the potential relative ship impacts. With this setup, the model performance and potential ship impact of the different models can be directly compared.

3.1.1 NO_2 Model Performance

Table 2 contains R, NMB and RMSE based on the annual time series for NO_2 at all stations. The highest correlation across all 62 stations showed LOTOS-EUROS followed by CMAQ with a slightly lower correlation (LOTOS-EUROS: R = 0.45; CMAQ: R = 0.42), whereas for CHIMERE, EMEP and CAMx, no to weak correlation was found (R = 0.08 to R = 0.10). The NMB suggests that all five CTMs underestimate the annual mean concentrations at most measurement sites; the NMB for all stations is negative for all models. The RMSE is within the same range for all models (RMSE = 15.6 µg/m³ to 19.5 µg/m³; Table 3).

Time series for three example stations show the temporal variations between measured and modeled data (Appendix C). The supplements provide an overview of the mean values of stations in each map parcel ("west", "north", "south", "east"; Supplement Figure S2). Figure C1 displays a time series at an urban background station in France (fr08614, "Gauzy", latitude: 43.8344, longitude: 4.374219), which was chosen because southern France will be investigated in greater detail as part of this study. Figure C2 shows a rural background station in Italy (it1773a, "Genga – Parco Gola della Rossa", latitude: 43.46806, longitude: 12.95222), which was chosen due to its central location in the domain and the high number of stations in Italy. Figure C3 displays the time series at a station in Greece (gr0035a, "Lykovrysi", latitude: 38.06963, longitude: 23.77689) to include a station in the eastern part of the domain.

Measurements at the French station show the highest NO_2 values in winter, with peaks between 40 µg/m³ and 55 µg/m³ (Figure C1). LOTOS-EUROS and EMEP underestimate the values throughout the year. Moderate correlation was calculated for CMAQ (R = 0.6) and LOTOS-EUROS (R = 0.65) at this station. The simulated ship impact has annual mean values from 0.2 µg/m³ (EMEP, CAMx) to 0.6 µg/m³ (CMAQ) at station fr08614. Shipping emissions have a potential relative impact between 1.8 % (EMEP) and 6.7 % (CMAQ) to the total concentration in the annual mean. The highest potential ship impact at this

station was modeled by CMAQ. At the Italian station, 1773a lower NO_2 concentrations were measured compared to the station in France. The highest peaks are approximately 20 µg/m³ in winter. At station it1773a, the potential ship impact to the total NO_2 concentration has annual mean values between 0.07 µg/m³ (LOTOS-EUROS) and 0.5 µg/m³ (CAMx). The highest relative potential ship impact was 7.9 % and was modeled by CAMx. At station gr0035a, the lowest simulated values are shown by CMAQ and LOTOS-EUROS. The highest values display EMEP at this station, also with the highest correlation between measured and simulated data (R = 0.55). The potential ship impact at the Greek station is between 5.0 % (EMEP) and 15.3 % (CAMx), which is higher than the potential ship impact at the other two stations.

All CTMs underestimate the actual measured total NO_2 values at both stations, except for LOTOS-EUROS in Italy. None of the models is able to model matching peak values. Neither at the station in France, Italy nor Greece models showed seasonal variation in concentrations, whereas NO_2 usually has higher values in winter and lower values in summer, mainly because of lower photolytical degradation and suppressed vertical mixing, as described, i.e., in Ordóñez (2005).

Differences in potential ship impacts between the stations are caused by the location and station type (fr08614 = urban background; it1773a = rural background; gr0035a = suburban background). At the French station, the traffic-related NO_2 concentration might supersede the ship-related NO_2. The station in Italy is not located in a city, so the NO_2 concentration caused by ships comes to the fore. The highest potential ship impact was simulated at the station in Greece because it is suburban but close to the Port of Piraeus, which is one of the largest ports in the Mediterranean Sea. As expected, the average potential ship impact is low at stations that are not directly located at the coast or to a harbor.

To compare the correlation R, NMB and RMSE at all measurement stations for all models, the results of the comparison are divided by country and displayed in boxplots (Figure 2). Each dot displays one measurement station. The correlation measured against the simulated annual mean NO_2 is highest for LOTOS-EUROS and CMAQ in all countries, reflecting the results shown in Table 3 for correlation. Nevertheless, boxplots for NMB and, in particular, for RMSE visualize that differences among countries are larger than differences among the models (Figure 2 b, c). This means that all models show good or bad performance at some stations, which was not found to be statistically relevant.

Underestimations by models of NO_2 at urban sites were found in other studies (Karl et al., 2019a; Giordano et al., 2015), despite differences in grid size. Karl et al. (2019a) used a grid resolution of 4 km, and Giordano et al. (2015) used a grid resolution of ~ 0.25° (27 km to 28 km). The underestimation might be due to too low emissions in the inventory used by the models and the heterogeneity of emissions. Regional CTMs cannot display small-scale spatial heterogeneity; coarse grid cells are not representative of the measurement location. Giordano et al. (2015) suggested in their study that the underestimation of NO_2 could be caused by either an underestimation of the chemical lifetime of NO_x, excessively high dry deposition, an underestimation of natural emissions at rural and remote stations or a combination of these factors. Differences in radical concentrations and reactive nitrogen might be additional reasons for underestimation (Knote et al., 2015).

The model performance of NO_2 has shown that differences in time series between the models occur, caused by the differences in meteorology and large grid size. Large grid sizes can cause errors insofar as in simulations the land areas are not seen as such but as water areas. This is especially problematic when having measurement stations located close to the sea.

Table 3: Correlation, normalized mean bias (NMB), root mean square error (RMSE), observational (obs) and simulated (sim) mean values of NO_2 for 2015: first data were averaged station wise and then averaged for all 62 stations.

	Correlation R	NMB	RMSE (µg/m³)	sim (µg/m³)	obs (µg/m³)
CAMx	0.08	-0.32	19.5	8.1	
CHIMERE	0.10	-0.52	18.5	5.8	
CMAQ	0.42	-0.56	17.3	6.7	16.6
EMEP	0.10	-0.40	18.8	7.1	
LOTOS-EUROS	0.45	-0.52	15.6	7.6	

405

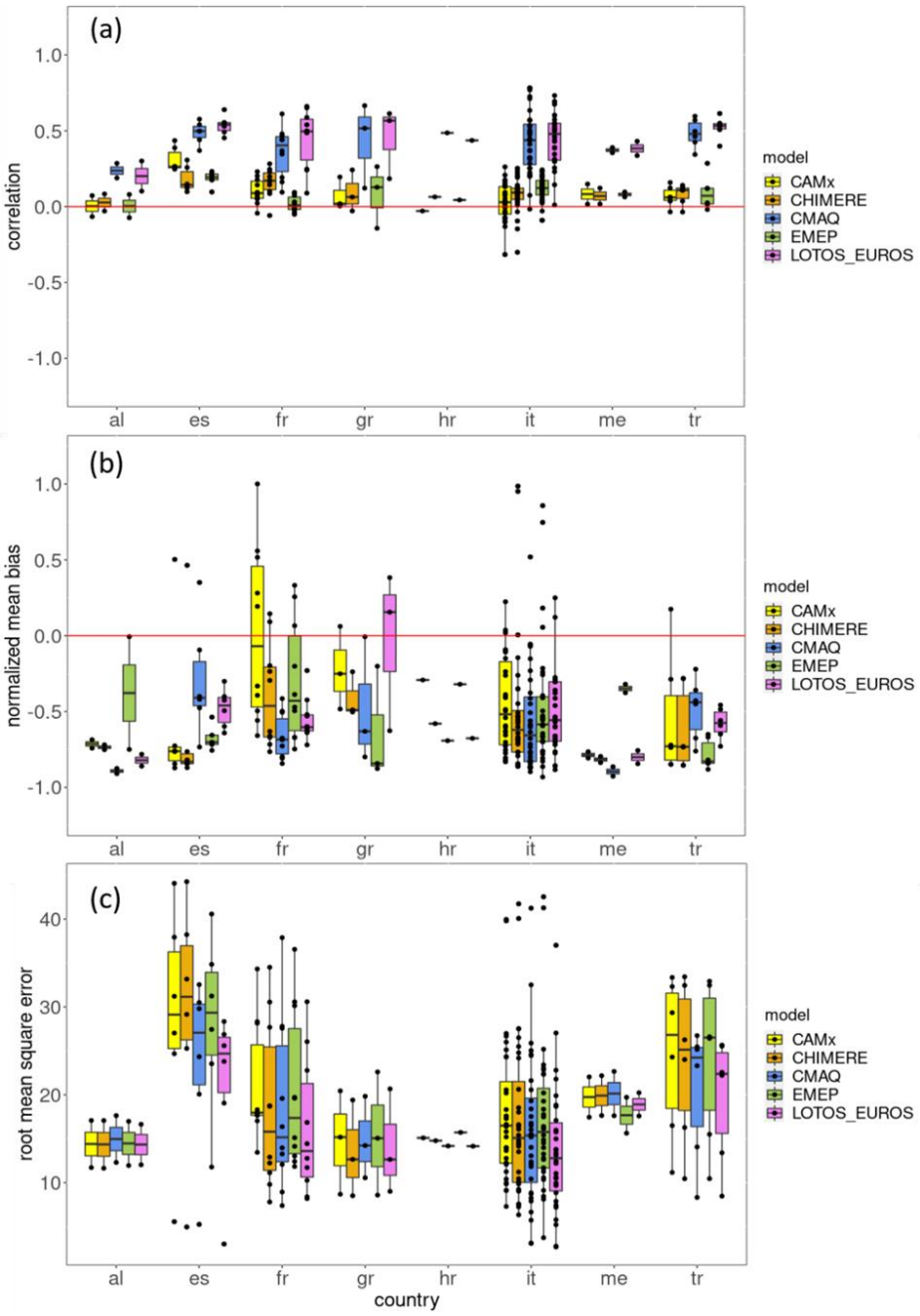

Figure 2: (a) = Correlation, (b) = NMB, (c) = RMSE for annual mean NO_2 concentration based on hourly data. Dots display annual mean values at measurement stations for the respective countries (al = Albania; es = Spain; fr =France; gr = Greece; hr = Croatia; it = Italy; me = Montenegro; tr = Turkey). Boxplots are for the models with the boxes displaying the interquantile range (IQR) between the 25th (Q1) and 75th (Q3) percentile, the black line displays the median (Q2), whiskers are calculated as Q1–1.5*IQR (minimum) and Q3 + 1.5*IQR (maximum).

3.1.2 NO_2 Spatial Distribution

The simulated annual mean NO_2 concentrations considering all emission sectors are similar for all CTMs, with most values between 0.0 µg/m³ and 2.0 µg/m³ (Figure 4). CAMx and CHIMERE have the largest areas, with values exceeding 5.0 µg/m³, especially along the main shipping routes and in urban areas. The CMAQ, EMEP and LOTOS-EUROS figures look similar, which is in good agreement with the displayed time series in Sect. 3.1., where the results are within the same range.

Over land area, all model simulations display a concentration pattern ranging within one order of magnitude. Nevertheless, the frequency distributions of the CMAQ, EMEP and LOTOS-EUROS simulations show the highest frequency between 1.0 µg/m³ and 2.0 µg/m³, whereas for CAMx and CHIMERE, they are more equally distributed. Higher values of NO_2 concentrations simulated by CAMx and CHIMERE might indicate a longer lifetime of NO_2 in the atmosphere. NO_2 reacts quickly with hydroxyl radicals (OH) and forms HNO_3, or NO_2 photolysis creates O_3 during the daytime. The annual mean HNO_3 concentrations are between 2.0 µg/m³ to 5.0 µg/m³ for CAMx and CHIMERE over water areas and are 0.8 µg/m³ to 2.0 µg/m³ over water areas for CMAQ, EMEP and LOTOS-EUROS (Supplement S11). Over land areas, the HNO_3 concentrations are within one range for all models. A lower HNO_3 concentration is expected for CTMs with longer lifetime of atmospheric NO_2. Nevertheless, there can be a misinterpretation when both concentrations are high. Therefore the data was normalized by using the HNO_3:NO_2 ratio (Supplements S12). Especially along the main shipping routes differences are displayed. There, values are lower in CAMx and EMEP compared to the other models. This can be explained by the lower HNO_3 formation by these models along the shipping routes.

Also the meteorology might influence the vertical mixing of NO_2. This leads to differences between the models or explains the similarity between CAMx and CHIMERE due to the usage of the same meteorology. Nevertheless, this point will not discussed here in detail since in the present study only the lowest layer was considered and the vertical mixing processes were not evaluated.

The correlation between the models for total NO_2 concentration was calculate based on hourly data (Table 4). The highest correlation was found between CAMx and CHIMERE (R = 0.80). Weak correlations were found between LOTOS-EUROS and CAMx (R = 0.31) and LOTOS-EUROS and CHIMERE (R = 0.36). This weak correlation is due to the differences in frequency distribution, with LOTOS-EUROS showing most values below 1.0 µg/m³, whereas for CAMx and CHIMERE, more values are located in the higher value ranges. Overall, the models can give a robust estimate regarding the base run of the annual mean of NO_2.

The highest potential impact of ships to total NO_2 concentrations was found at the main shipping routes, with values > 85 % (Figure 5). Similar values were found for the Baltic Sea (Karl et al., 2019a) and for the Iberian Peninsula (Nunes et al., 2020). CHIMERE and CAMx model the highest values over the sea region, with a potential ship impact to NO_2 between 60 % and 85 %. CMAQ, LOTOS-EUROS and EMEP have similar patterns for ship impacts over the sea.

On the Mediterranean coastline, CMAQ, CHIMERE, LOTOS-EUROS and EMEP simulate a similar potential impact, with 25 % to 45 % potential ship impacts to total NO_2. Merico et al. (2017) found similar results in a study with NO_2 shipping

impact up to 32.5 % regarding four port-cities in the Adriatic-Ionian Sea. CAMx reveals a higher impact with > 85 % at the coastline. The potential ship impact displayed in the time series in Sect. 3.1 was lower, although the measurement stations were not far from the coast. This shows that although the potential impact from ships reaches regions far from the coast, the highest impact is over the sea area. The frequency distribution for the relative ship impact shows that all models simulate most values between 0 % and 5.0 % of the ship potential impact. Interestingly, the distribution is lowest at values between 20 % and 40 % (CMAQ, EMEP, LOTOS-EUROS) and 60 % (CAMx, CHIMERE) and then increases again at higher values, showing a bimodal distribution. This is due to large areas with high potential impacts over water and large areas with low potential impacts over land or near harbors.

Over land in the northeast area of the domain, slightly negative potential ship impacts are derived from the CMAQ, CAMx, LOTOS-EUROS and EMEP results. CHIMERE shows only very few negative values, but in the same region. Negative potential ship impacts to NO_2 concentrations may arise when the zero-out method is applied. They are a consequence of the nonlinear NO_x gas phase chemistry. Especially in areas where the impact of NO_x emissions from shipping is very low, less NO oxidation takes place because the additional NO from shipping in other areas already consumed the oxidants (e.g. O_3).

The boxplots in Figure 3 display the annual mean values for the whole model domain of NO_2. Model results vary for the base run but also for the potential ship impact. This variability needs to be taken into account when the predictive power of CTMs is considered. The “all_mean” boxplot displays the mean of all models and displays that in comparison with other models, CAMx has high values. It further helps to show which CTM tends to simulate higher or lower values compared to others. The “all_mean” boxplots show similar ranges as boxplots for CMAQ and EMEP, particularly regarding absolute and relative potential ship impacts. Additionally, models simulating a higher overall concentration of pollutants also tend to simulate a higher potential ship impact. The relative potential ship impact is highest for CAMx and CHIMERE and lowest for LOTOS-EUROS.

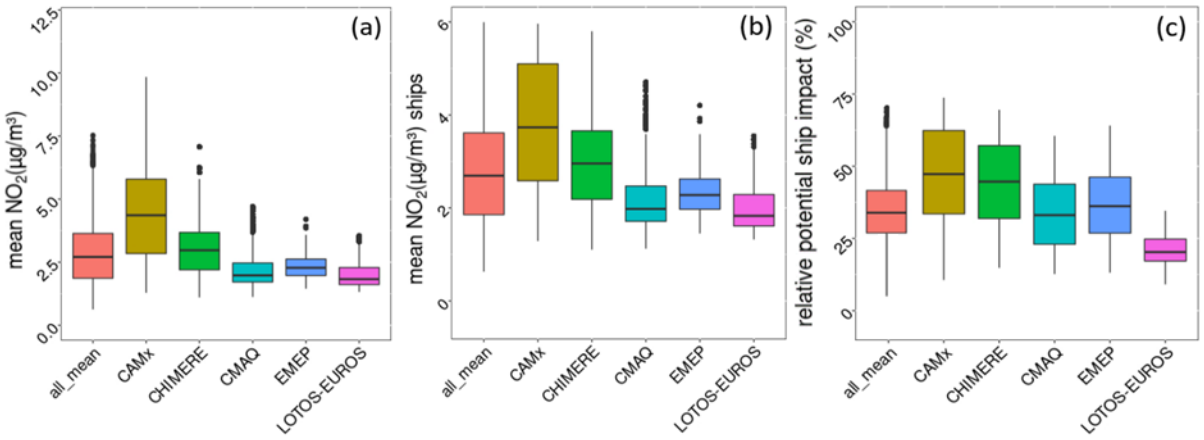

Figure 3: Annual mean for all grid cells in the whole model domain. (a) = mean NO_2 for all emission sectors (base case), (b) = mean NO_2 for shipping only, (c) = relative potential ship impact to total NO_2 concentration. All_mean is the mean value of all models, with a median of (a) = 2.8 µg/m³, (b) = 0.7 µg/m³ and (c) = 27.7 µg/m³.

Table 4: Correlation for the NO_2 base run between models for the whole domain (all grid cells), based on hourly data for NO_2 total concentration.

all	CAMx	CHIMERE	CMAQ	EMEP	LOTOS-EUROS
LOTOS-EUROS	0.31	0.36	0.71	0.73	-
EMEP	0.39	0.44	0.73	-	
CMAQ	0.39	0.43	-		
CHIMERE	0.80	-			
CAMx	-				

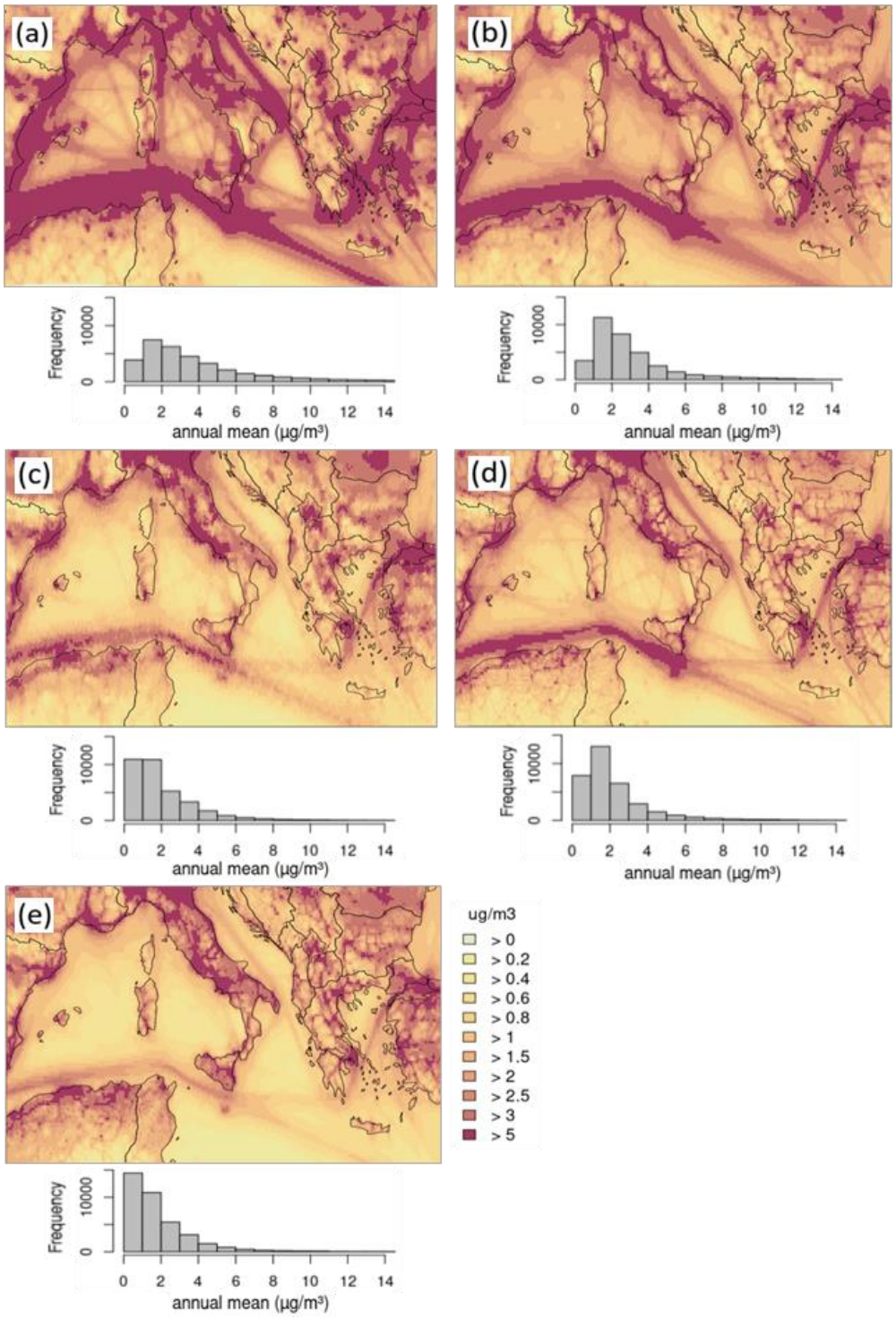

Figure 4: Annual mean NO_2 total concentration. (a) = CAMx, (b) = CHIMERE, (c) = CMAQ, (d) = EMEP, (e) = LOTOS-EUROS. Below the domain figure is the respective frequency distribution displayed for the annual mean NO_2 concentration, referred to the whole model domain.

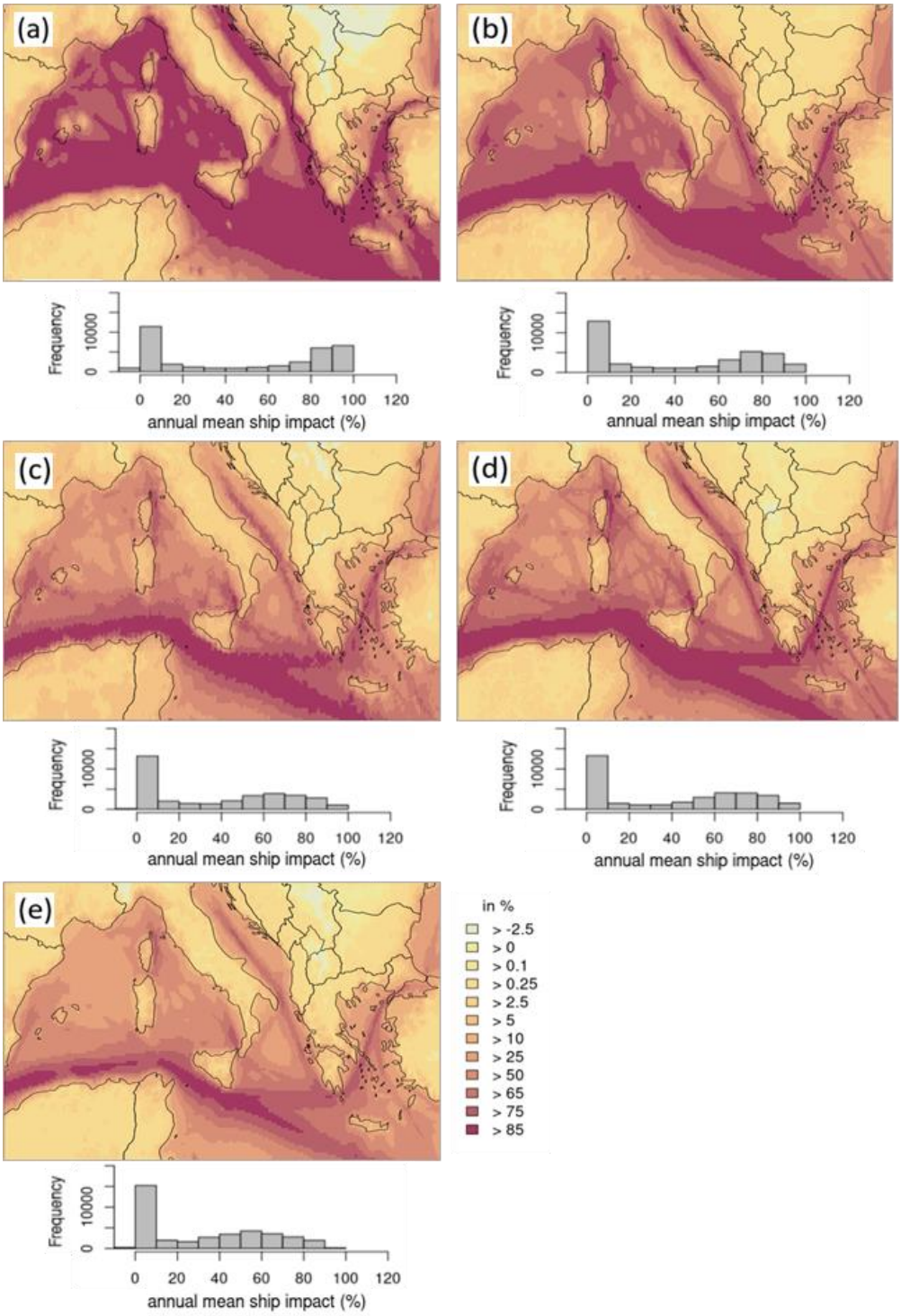

Figure 5: Annual mean NO_2 potential ship impact. (a) = CAMx, (b) = CHIMERE, (c) = CMAQ, (d) = EMEP, (e) = LOTOS-EUROS. Below the domain figure is the respective frequency distribution displayed for the annual mean NO_2 potential ship impact, referred to the whole model domain.

3.1.3 O_3 Model Performance

The tropospheric O_3 concentrations are strongly connected to the NO_2 concentration and to the oxidized nitrogen chemistry in the atmosphere. O_3 can be both an initiator and a product of photochemistry; thus, it is crucial in tropospheric chemistry.

Simulated versus measured data of one-year daily mean O_3 time series show a weak (EMEP: R = 0.38) to moderate correlation (CAMx: R = 0.40; CHIMERE: R = 0.47; CMAQ: R = 0.60; LOTOS-EUROS: R = 0.69; Table 5).

Selected time series represent these differences in correlation (Appendix D). Nevertheless, for the first months of the year CHIMERE, CAMx and CMAQ overestimate the actual measured O_3 values (Figure D1: station fr08614; Figure D2: station it1773a; Figure D3: gr0035a).

During summer months, O_3 shows the highest values due to increased photochemical activity. The simulated potential ship impact is between 1.1 µg/m³ (CAMx) and 2.8 µg/m³ (LOTOS-EUROS) at station fr08614 and has a relative potential impact between 1.3 % (CAMx) and 4.0 % (CHIMERE) to the total concentration. At station it1773a, the mean O_3 potential ship impact is between 1.0 µg/m³ (CAMx) and 3.0 µg/m³ (CHIMERE), and the relative potential impact ranges from 1.1 % (CAMx) to 3.5 % (LOTOS-EUROS). The potential ship impact of station gr0035s ranges from -0.1 µg/m³ (CAMx) to 3.7 µg/m³ (CMAQ; LOTOS-EUROS), which is a relative potential impact of -0.1 % (CAMx) and 3.7 % (CMAQ).

The O_3 potential ship impact is within the same range at both stations and for all five CTMs. Figure 6 shows that CMAQ has the smallest bias compared to the other models (NMB = 0.28), followed by LOTOS-EUROS (NMB = 0.36). The RMSE is lowest for CMAQ (RMSE = 31.2 µg/m³) and LOTOS-EUROS (RMSE = 32.6 µg/m³), along with the lower NMB compared to the other models. The performance analysis revealed that all five models predict higher O_3 concentrations than those measured at almost all stations (NMB > 0). The overestimation of actual measured O_3 by the models is in line with results from previous studies (Karl et al., 2019a; Appel et al., 2017; Im et al., 2015a; Im et al., 2015b). Im et al. (2015a) showed that O_3 concentrations above 140 µg/m³ are underestimated, while concentrations below 50 µg/m³ are overestimated by 40 % to 80 % in all considered models. This overestimation of O_3 by the models is likely linked to the chemical boundary conditions used in the regional CTMs. Analyses of the boundary conditions revealed that, especially in winter, O_3 levels are mostly driven by transport instead of local production due to limited photochemistry (Giordano et al., 2015).

CHIMERE uses boundary conditions from monthly mean climatologies simulated with the LMDz-INCA model, CAMx uses Mozart-4 output, LOTOS-EUROS and CMAQ use IFS-CAMS reanalysis data and the EMEP model uses ozone boundary conditions provided with the open source model distribution for 2015. These differences in input for the boundary conditions can be seen as the reason for the varying results in O_3 (Supplements S13 to S16).

All CTMs performed relatively well and are able to represent the course of the year, with higher values in summer and lower values in winter. Nevertheless, in some cases, the values in spring are overestimated.

Table 5: Correlation, normalized mean bias (NMB), root mean square error (RMSE), observational (obs) and simulated (sim) of O_3 as the mean values for 2015: the first data were averaged station wise and then averaged for all 48 stations.

	Correlation R	NMB	RMSE (µg/m³)	sim (µg/m³)	obs (µg/m³)
CAMx	0.40	0.41	40.5	90.4	66.5
CHIMERE	0.47	0.57	45.4	100.7	
CMAQ	0.60	0.28	31.2	82.2	
EMEP	0.38	0.37	39.0	87.6	
LOTOS-EUROS	0.69	0.36	32.6	87.7	

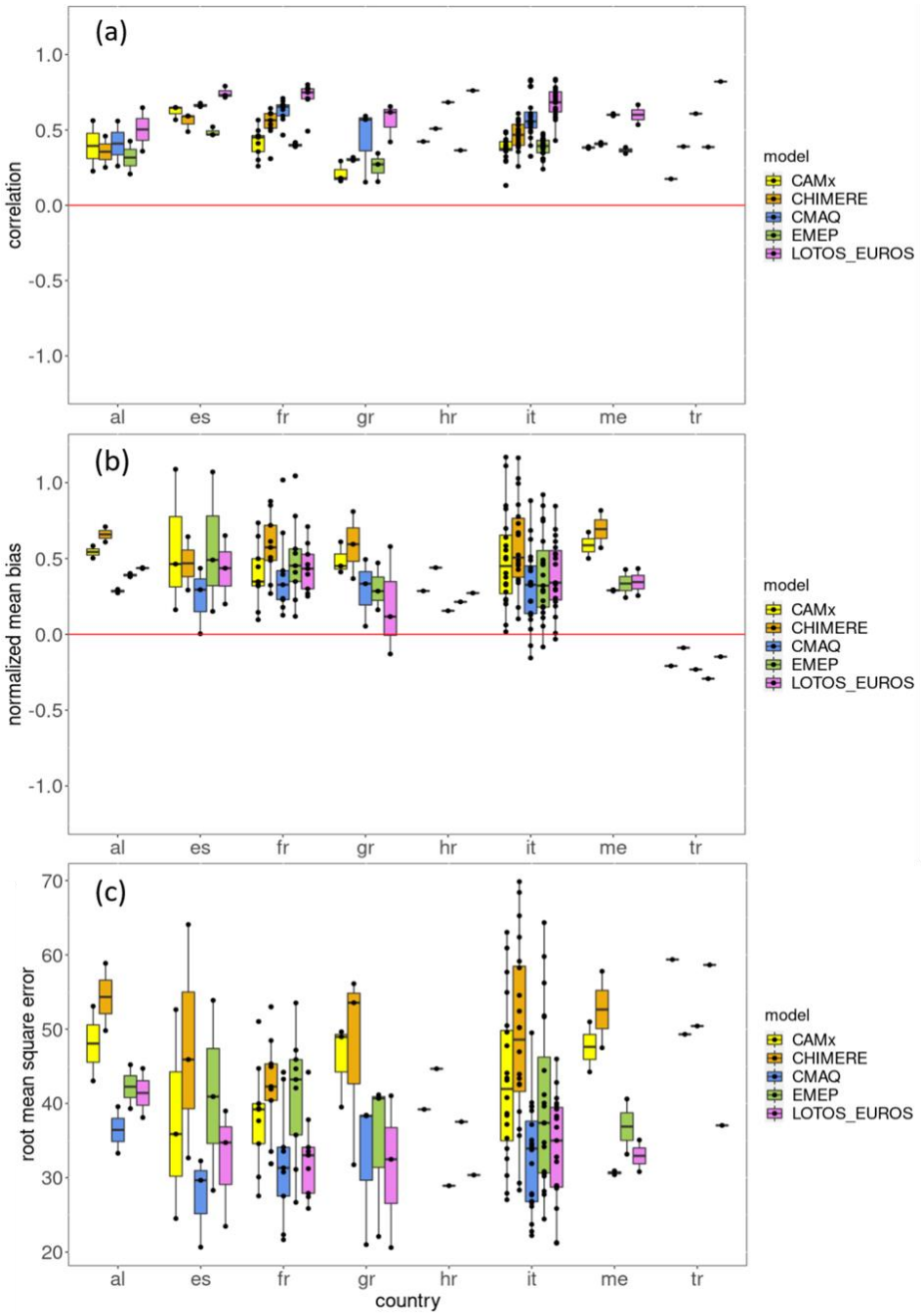

Figure 6: (a) = Correlation, (b) = NMB, (c) = RMSE for annual mean O_3 concentration. Dots display values at measurement stations for the respective countries (al = Albania; es = Spain; fr =France; gr = Greece; hr = Croatia; it = Italy; me = Montenegro; tr = Turkey). Boxplots are for the models with the boxes displaying the interquantile range (IQR) between the 25th (Q1) and 75th (Q3) percentile, the black line displays the median (Q2), whiskers are calculated as Q1–1.5*IQR (minimum) and Q3 + 1.5*IQR (maximum).

3.1.4 O_3 Spatial Distribution

The annual mean concentration of O_3 considering all emission sectors is between 60 µg/m³ and 120 µg/m³ for all models (Figure 8). This is consistent with the measurements displayed in the time series in Sect. 3.2.1. CHIMERE, CAMx and LOTOS-EUROS show particularly high O_3 concentrations over the sea. Interestingly, EMEP results are similarly high over the sea area, but in comparison with other CTMs, concentrations are lower over land, and even values below 60 µg/m³ can be seen in the Po valley (Figure 8, d). Regarding the correlation between the models for total concentration over the whole domain, it is highest between CMAQ and EMEP (R = 0.71) and lowest for CAMx and LOTOS-EUROS (R = 0.42), but predominantly moderate correlations were found among the models (Table 6).

In general, all CTMs show high annual mean concentrations over the sea areas and low annual mean concentrations over land areas.. This is due to lower dry deposition over sea and the overall higher emissions over land. Furthermore, high values of O_3 are expected to enter the domain from the eastern part of the Mediterranean Sea. This point will be discussed in Sect. 4. The frequency distribution of the annual mean total concentration of O_3 has a bimodal distribution for CHIMERE, CMAQ and EMEP. This reflects photochemical O_3 depletion or production, with high values over water areas and lower values over land. Over water, low O_3 depletion is expected during the night. A comparison of diurnal cycles of O_3 over water and over land shows that this presumption is reflected by CMAQ and EMEP results, showing more pronounced cycles of O_3 in grid cells over land (Supplements S17). However, the diurnal cycles of CAMx, CHIMERE and LOTOS-EUROS do not show differences in amplitude over land and water. Despite this, over water, all models show a higher spread of values within diurnal cycles, displaying that there is more variability in the course of the year over water than over land.

The potential relative impact of ships to total O_3 concentrations is lowest in areas with a high potential impact of shipping to total NO_2 (Figure 9). It decreases to -20 % in areas with high NO_2 concentrations in all model results, displaying a local scale titration of O_3 by NO, which is emitted by ships. This reverse relationship between NO_2 and O_3 was already shown in other studies (e.g., Karl et al., 2019b). Measurement studies also indicate that emissions of NO lead to local reduction of O_3 concentration and showed that there could be an increase at larger distances (Merico et al., 2016). Consequently, the largest areas with O_3 destruction for the CAMx and CHIMERE coincide with areas where the models show the highest potential impact of shipping to NO_2. The comparison with the time series shows the highest potential ship impact to the total O_3 concentration in summer. Likewise, in Sect. 3.1.4 lowest potential ship impact was found for CAMx.

Figure 7 shows boxplots with annual mean values of the models for the whole domain. It shows that CAMx, CHIMERE and LOTOS-EUROS are within one range regarding the annual mean total concentration. The CMAQ and EMEP simulations are lowest for the annual mean O_3 total concentration. Regarding potential ship impact, all CTMs except CAMx are within one range.

The present study does not contain the parts of the Mediterranean Sea furthest east due to the focus of the project on the western Mediterranean Sea with its harbor cities as well as due to the limited extent of the WRF domain. A more detailed investigation of the boundary conditions of CMAQ has shown high O_3 values in the eastern part of the domain. A high O_3 production over

the eastern Mediterranean Sea and a steep west-east gradient of O_3 were described in previous studies (i.e., Doche et al., 2014; Safieddine et al., 2014; Liu et al., 2009). This production influences the amount of O_3 in the western part of the Mediterranean Sea. Safieddine et al. (2014) found an increase of up to 22 % in O_3 in the eastern part of the Mediterranean basin compared to the middle of the basin. Doche et al. (2014) described a steep west–east O_3 gradient with the highest concentrations over the eastern part of the Mediterranean basin.

Overall, all models showed a relatively good performance for O_3 but differed in simulating spatial distribution and potential ship impact mainly over water. Although boxplots for annual mean values of O_3 differ, for relative potential ship impact they show that CHIMERE, CMAQ, EMEP and LOTOS-EUROS are within one range. Diurnal cycles did not reveal differences in O_3 depletion over water and land among the models.

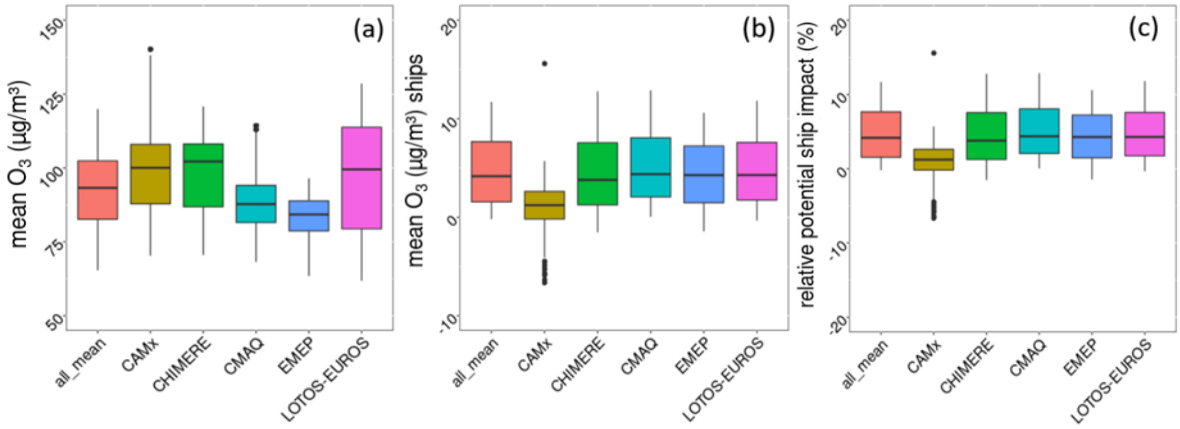

Figure 7: Annual mean for the whole model domain. (a) = mean O_3 for all emission sectors (base case), (b) = mean O_3 for shipping only, (c) = relative potential ship impact to total O_3 concentration. All_mean is the mean value of all models, with a median of (a) = 92.4 µg/m³, (b) = 4.0 µg/m³ and (c) = 4.2 µg/m³.

Table 6: Correlation between models for the whole domain (all grid cells) based on hourly data for O_3 total concentration.

all	CAMx	CHIMERE	CMAQ	EMEP	LOTOS-EUROS
LOTOS-EUROS	0.42	0.59	0.58	0.59	-
EMEP	0.44	0.58	0.71	-	
CMAQ	0.50	0.56	-		
CHIMERE	0.63	-			
CAMx	-				

560

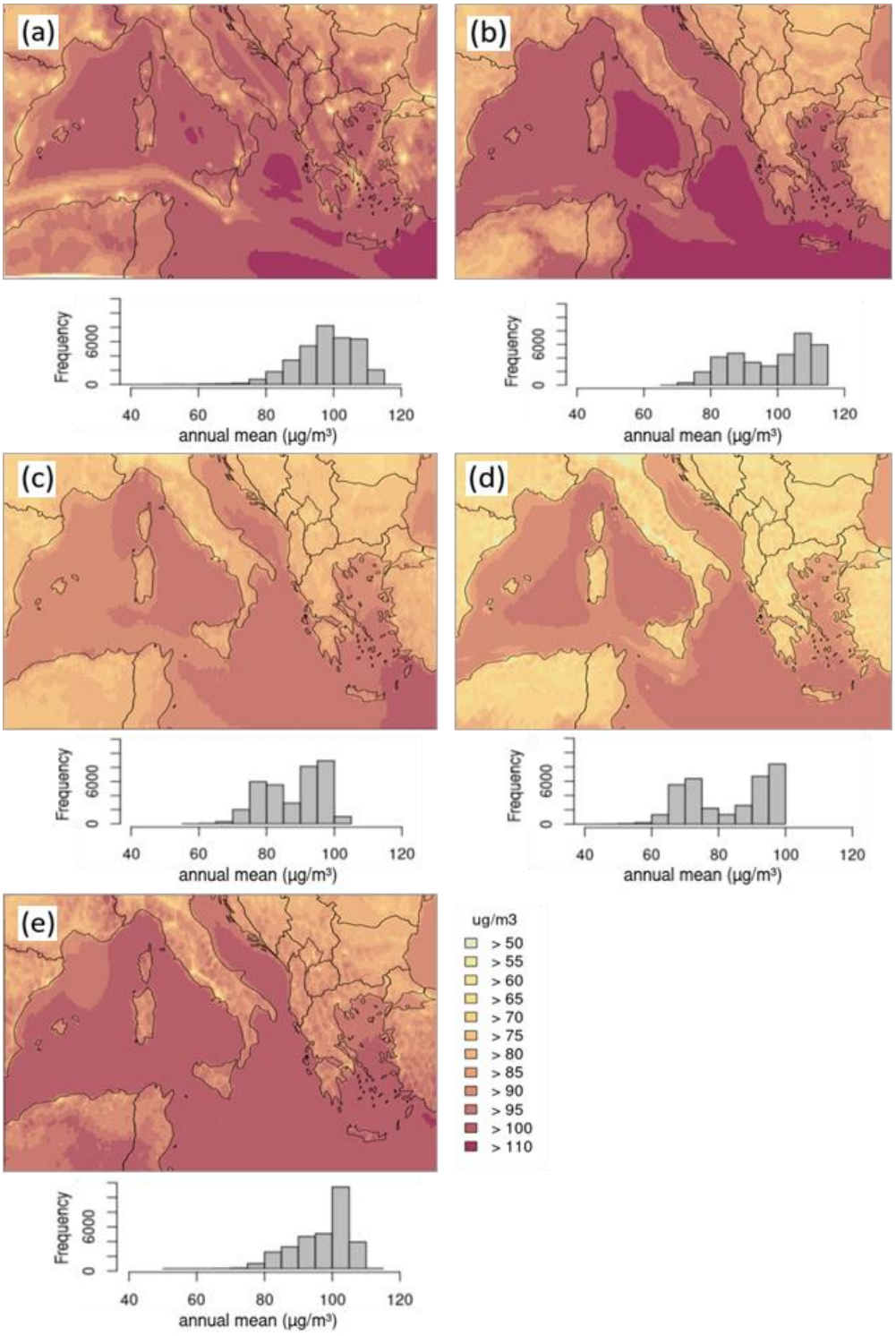

Figure 8: Annual mean O_3 total concentration. (a) = CAMx, (b) = CHIMERE, (c) = CMAQ, (d) = EMEP, (e) = LOTOS-EUROS; emisbase spatial distribution, annual mean value, white areas contain values below 60 µg/m³. Below the domain figure is the respective frequency distribution displayed for the annual mean O_3 concentration, referred to the whole model domain.

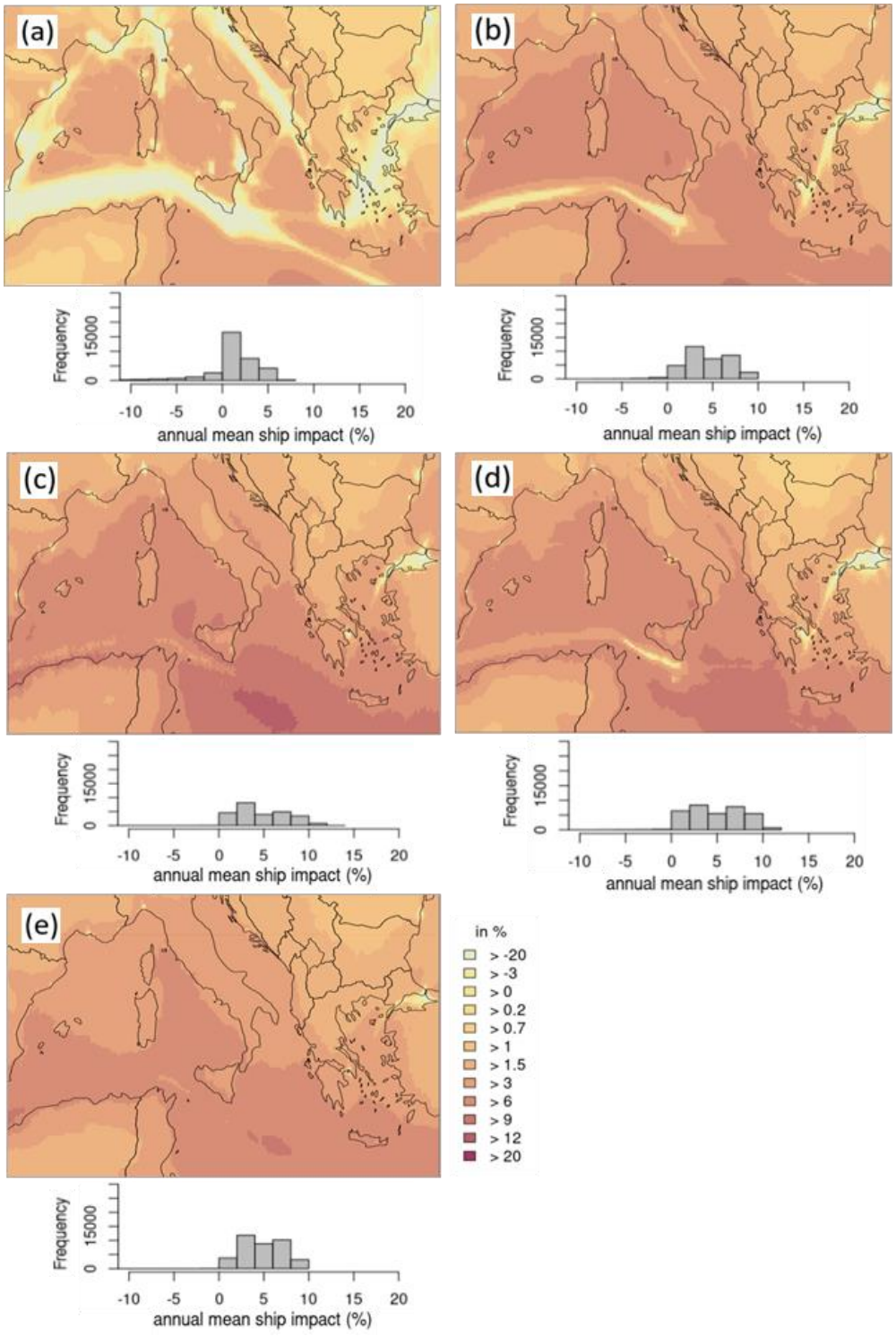

Figure 9: Annual mean O_3 potential ship impact. (a) = CAMx, (b) = CHIMERE, (c) = CMAQ, (d) = EMEP, (e) = LOTOS-EUROS; white areas display values below -20 %. Below the domain figure is the respective frequency distribution displayed for the annual mean O_3 potential ship impact, referred to the whole model domain.

3.2 O_x Spatial Distribution

The oxidation of VOCs produce O_3 in the troposphere when nitrogen oxides (NO; NO_2) and sunlight are present. Central to understanding this production is the photostationary state formed between NO, NO_2, and O_3 in sunlight. In emission-free air, a steady equilibrium would be expected; nevertheless, emission sources disturb this equilibrium. In areas with high NO emissions, O_3 destruction is expected, resulting in lower O_3 concentrations along the main shipping routes, in urban areas and in harbor cities.

The results show that all five CTMs tend to underestimate NO_2 and overestimate O_3, but at different magnitudes. For a better understanding of photochemical air pollution and chemical coupling, the oxidant levels ($O_x = O_3 + NO_2$) were calculated and displayed for all emission sources and for the potential ship impact. Clapp and Jenkin (2001) showed that the concentration of O_x levels can be described as a NO_x-independent regional impact, where the O_x impact equates to the O_3 background, and a NO_x-dependent local impact. The NO_x-dependent impact correlates with the primary pollution, coming from direct NO_2 emissions or VOC, which promote conversion from NO to NO_2 (Clapp and Jenkin, 2001).

In comparison with the O_3 spatial distribution and frequency distribution, the annual mean concentration of O_x displays a similar pattern between the results (Figure 10). As it was the case for O_3, CHIMERE and CAMx show the highest values over the sea area, and EMEP shows the lowest values over land areas. The frequency distribution shows bimodal distributed values for CHIMERE, CMAQ and EMEP, as for O_3. Thus, O_x levels are mainly NO_x-independent.

Nevertheless, NO_x-dependent O_x formation can also be seen in the potential ship impact to the total O_x concentration (Figure 11). The relative potential impact of O_x displays how much substances from ships are added to the atmosphere. O_x shows a strong conversion of NO_2 and O_3, thus the shipping lanes are no longer visible. High O_x potential impacts over water areas for CHIMERE, CMAQ, EMEP and LOTOS-EUROS indicate the local potential impact from shipping emissions (NO_2 and VOC), which cause high O_x levels in these areas. For CAMx, the O_x potential impact was lower.. This might be traced back to the overall higher concentration of NO_2 and O_3 in CAMx, leading to a lower proportion of other substances. Also, the differences between the O_x results among the models can occur due to the difference in O_3 that in turn results from the input from the boundaries. Here, CAMx displays an overall high input of O_3 from the boundary.

3.3 NO_x Spatial Distribution

To gain further insight into the differences in the lifetime of NO_2 in the models, NO_x (= NO + NO_2) was calculated and displayed (Appendix E). Differences in NO_x give a hint on the lifetimes because of the reaction of NO_2 with OH to HNO_3. The latter forms ammonium nitrate aerosol together with ammonia; thus, NO_2 is no longer in the gaseous phase. Another explanation is the dry deposition of NO_2, which also causes a loss and consequently differences in the NO_x pattern due to different deposition mechanisms. The spatial distribution of the annual mean NO_x and potential ship impact to the total NO_x concentration have shown a very similar pattern as for NO_2. The values of CAMx and CHIMERE are within one range, displaying higher values compared to CMAQ, EMEP and LOTOS-EUROS. These three models show results within one range.

To see the chemical fate of NO_2 the dry deposition could give a hint and will be considered in the following Sect 3.4.

595

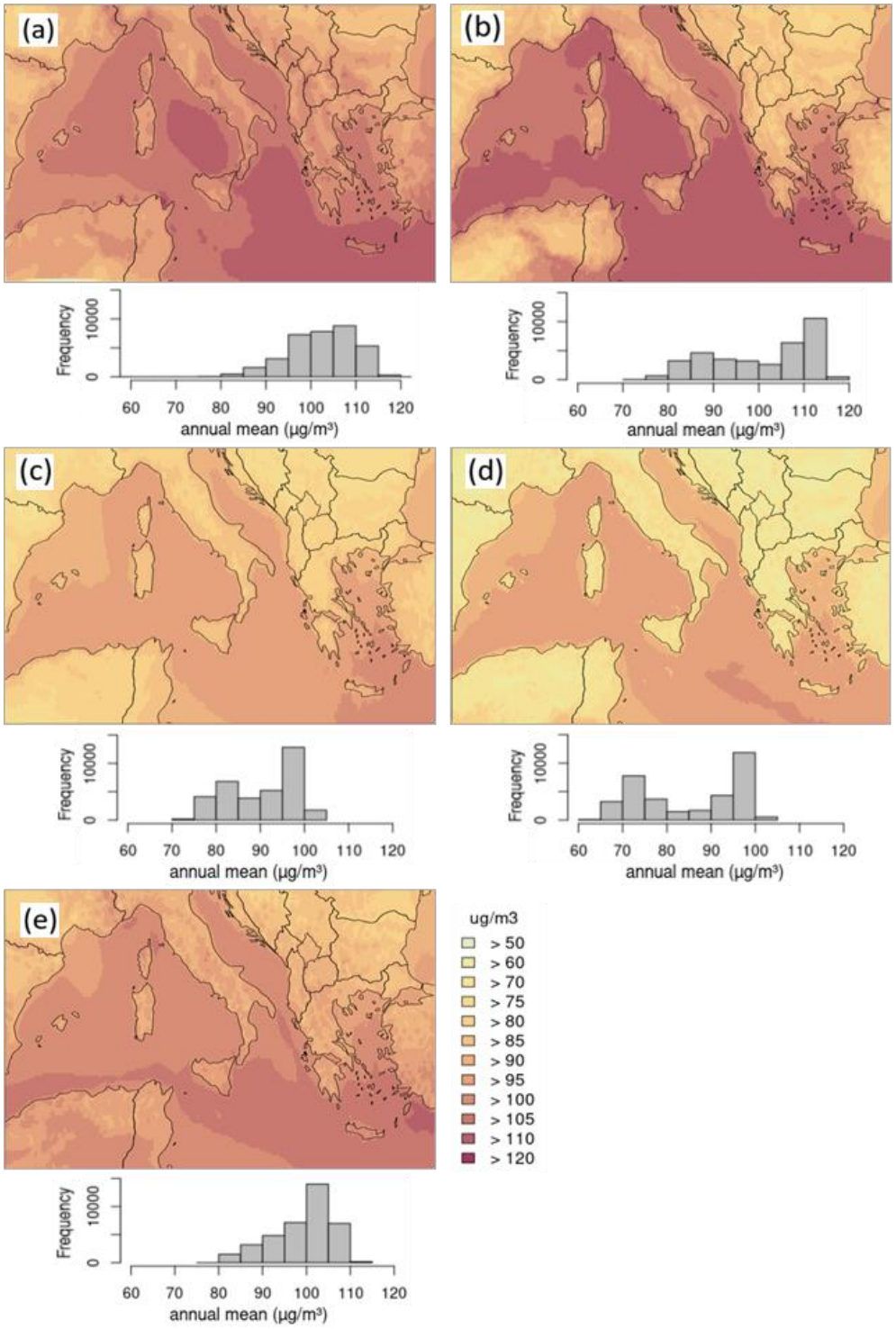

Figure 10: Annual mean O_x (= NO_2 + O_3) concentration. (a) = CAMx, (b) = CHIMERE, (c) = CMAQ, (d) = EMEP, (e) = LOTOS-EUROS. Below the domain figure is the respective frequency distribution displayed for the annual mean O_x concentration, referred to the whole model domain.

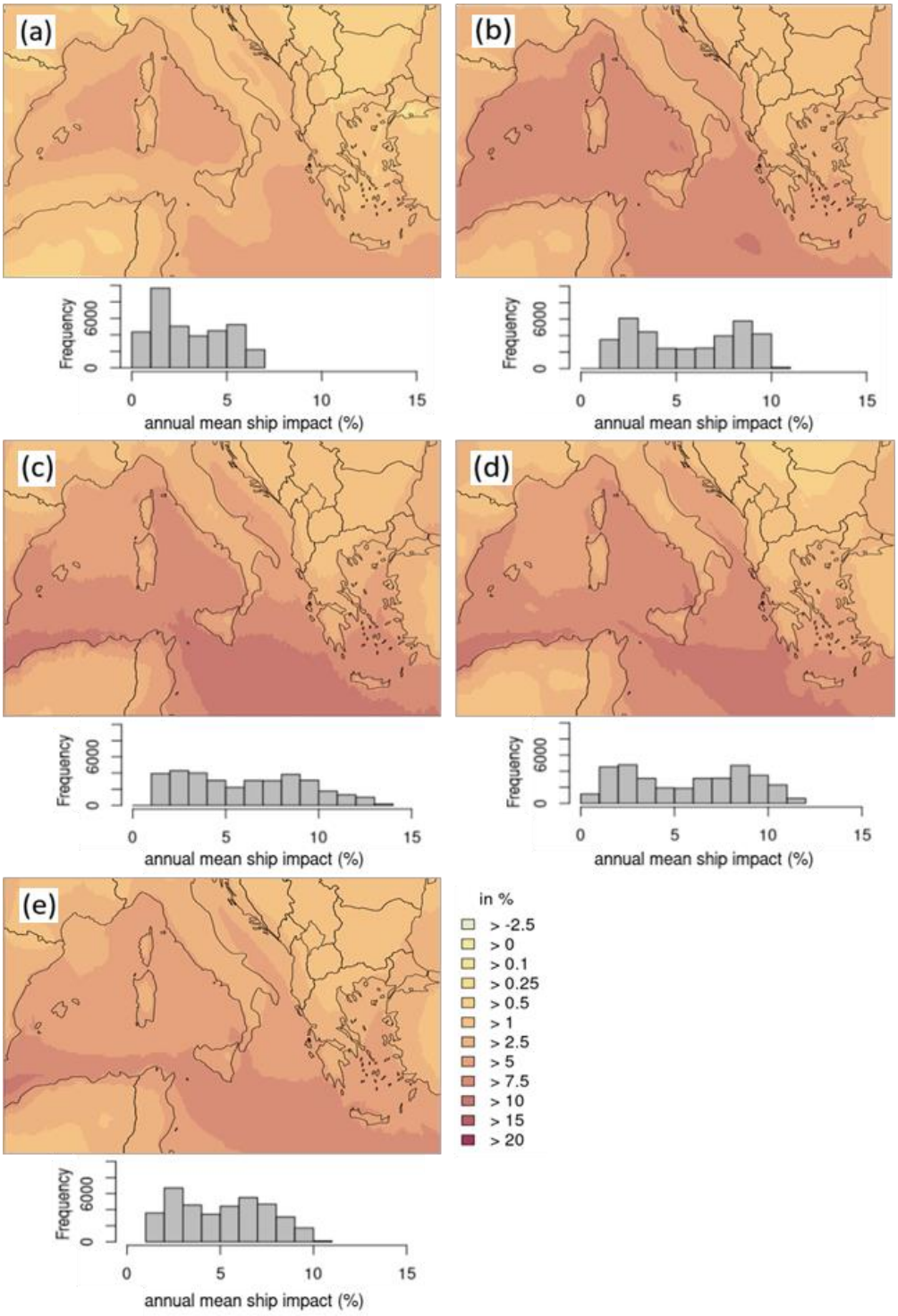

Figure 11: Annual mean O_x (= NO_2 + O_3) potential ship impact. (a) = CAMx, (b) = CHIMERE, (c) = CMAQ, (d) = EMEP, (e) = LOTOS-EUROS. Below the domain figure is the respective frequency distribution is displayed for the annual mean O_x potential ship impact, referred to the whole model domain.

3.4 Dry Deposition

In the present study, dry deposition of NO_2 and O_3 are displayed for the base and the no ship case for CAMx, CHIMERE, CMAQ and LOTOS-EUROS. EMEP does not deliver separate NO_2 and O_3 deposition files but does deliver oxidized and reactive nitrogen. Thus, EMEP is not considered in this chapter.

3.4.1 Dry Deposition of NO_2

The annual mean NO_2 dry deposition of all four compared CTMs displays similar values over land areas (Figure 12). In cities and densely populated regions, all models show high NO_2 dry deposition, with values over 300 mg/m²/year. Nevertheless, the frequency distribution of all values shows that this is mainly the case for CAMx and LOTOS-EUROS. Additionally, over the sea, the pattern of annual mean dry deposition of NO_2 is also similar for CAMx and LOTOS-EUROS.

Table 7 shows that the correlation was strongest between CHIMERE and CAMx (R = 0.72). Similarities and strong correlations in the output of both models were also found for the NO_2 concentration in Section 3.1.2. This can be traced back to the same meteorology data that were used by both CTMs.

The relative potential ship impact to the annual dry deposition of NO_2 is displayed in Figure 13. The lowest potential ship impact to NO_2 dry deposition is simulated by CMAQ and LOTOS-EUROS. In particular, CMAQ shows large areas with negative (-2.5 %) potential ship impacts over land. The CHIMERE simulations looks similar to the CAMx simulations over land. Along the coastline, CMAQ and LOTOS-EUROS show a potential impact of ships between 10 % and 25 %; CAMx and CHIMERE expect a potential ship impact to the total annual deposition of 25 % to 75 %. The highest potential impact is displayed by CAMx.

Differences in NO_2 dry deposition model results can be due to the dry deposition velocities but also due to the different meteorology data used by the models (Wichink Kruit et al., 2014). Dry deposition velocities of NO_2 (Supplements S18) display that deposition velocities of CHMIERE and CMAQ are within one range and are lower compared to CAMx and LOTOS-EUROS deposition velocities. Velocities of the latter two are within one range. High velocities might lead to higher deposition rates, leading to high annual mean deposition. This is reflected in the annual dry deposition of NO_2, where CAMx and LOTOS-EUROS simulate highest values. Overall, the models have more differences in NO_2 dry deposition than in air concentration. As was the case for NO_2 concentration, CAMx simulated the highest values in dry deposition. The lowest values in NO_2 dry deposition are displayed by CMAQ. In addition, the correlation between CMAQ and the other models was lowest.

High NO_2 deposition over water areas caused by ships contributes to eutrophication (Vivanco et al., 2018). A study by Im et al. (2013) showed values of approximately 500 kg (N) m^{-2} per year (≙ 50000 mg/m²/year) over the Mediterranean Sea, which means an exceedance of the critical load of 2 g to 3 g (N) m^{-2} per year (≙ 2000 to 3000 mg/m²/year) to marine and coastal habitats (Bobbink and Hettelingh, 2011). The present study focused on NO_2 dry deposition; thus, a direct comparison with critical load levels or with other studies regarding total N deposition would not be possible. A subsequent calculation of N showed that the simulated values in the present study do not exceed the critical loads (Appendix F). Nevertheless, NO_2 dry

deposition from ships contributes to the total N deposition budget, thus increasing with ship traffic and impacting the ecosystems in the Mediterranean Sea.

Table 7: Correlation between models for the whole domain (all grid cells) based on daily data for NO_2 total dry deposition.

all	CAMx	CHIMERE	CMAQ	LOTOS-EUROS
LOTOS-EUROS	0.48	0.55	0.22	-
CMAQ	0.22	0.27	-	
CHIMERE	0.72	-		
CAMx	-			

635

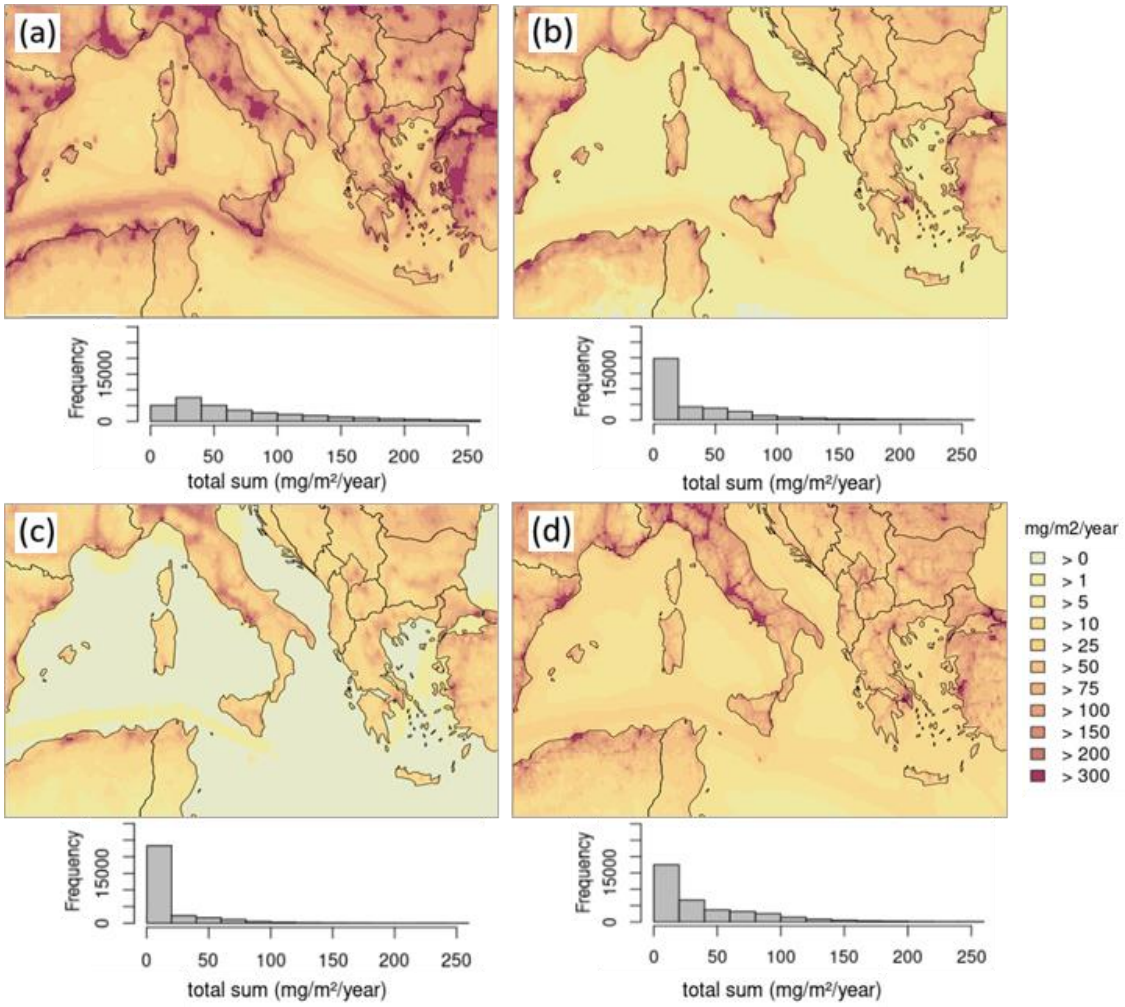

Figure 12: Annual total dry deposition of NO_2. (a) = CAMx, (b) = CHIMERE, (c) = CMAQ, (d) = LOTOS-EUROS. Below the domain figure is the respective frequency distribution displayed for the annual mean NO_2 dry deposition, referred to the whole model domain.

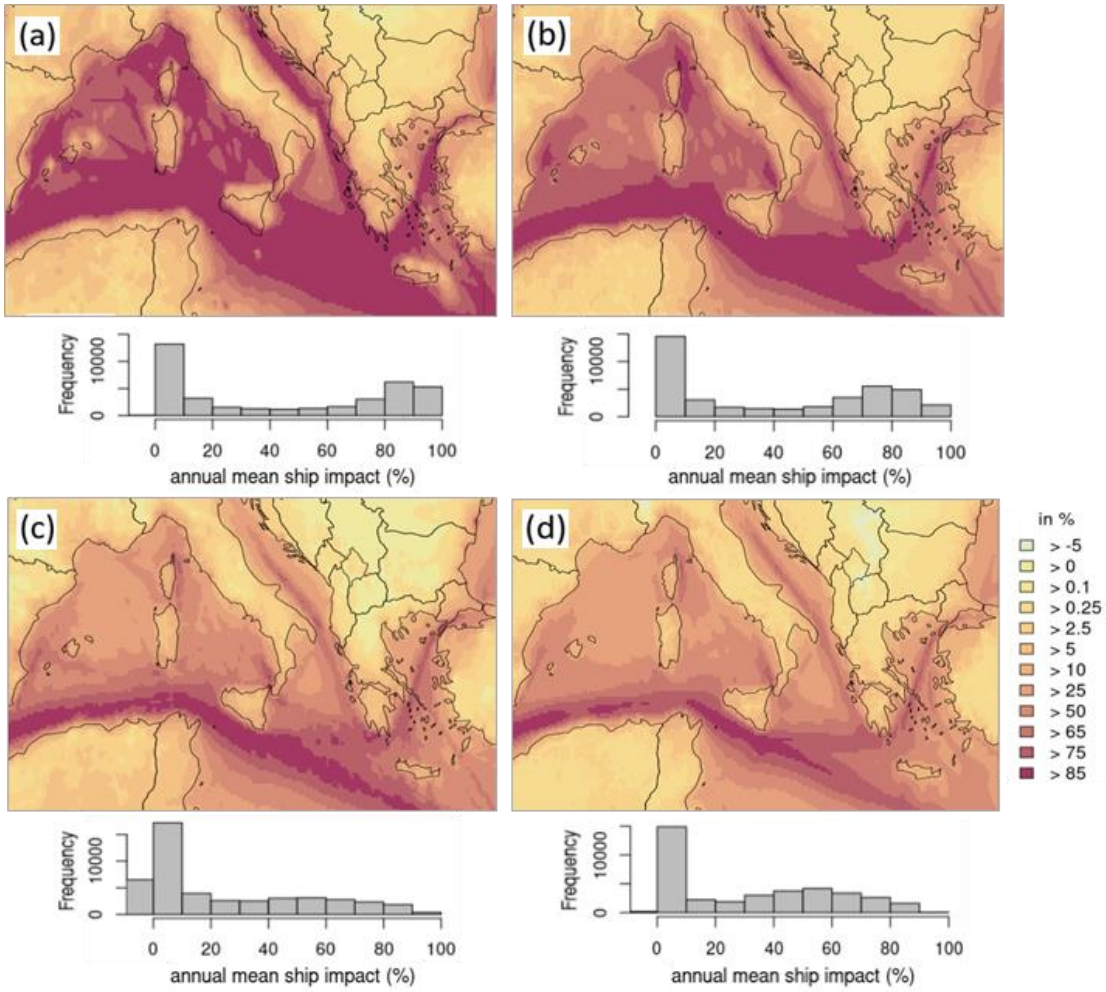

Figure 13: Annual mean dry deposition of NO_2 relative potential ship impact. (a) = CAMx, (b) = CHIMERE, (c) = CMAQ, (d) = LOTOS-EUROS. Below the domain figure is the respective frequency distribution displayed for the annual mean NO_2 dry deposition potential ship impact, referred to the whole model domain.

3.4.2 Dry Deposition O_3

Dry deposition is a major sink for O_3 in the lowest model layer. O_3 has high destruction rates on vegetated surfaces through plant stomata and lower rates on surfaces such as water or snow (Clifton et al., 2020). Spatial patterns of annual total O_3 dry deposition confirm this distribution. Over sea annual totals are lower (250 mg/m²/year to 1000 mg/m²/year) compared to values over land (2500 mg/m²/year to 10000 mg/m²/year; Figure 14). The correlation for the annual total concentration of O_3 dry deposition is highest between CHIMERE and CAMx, showing a moderate correlation (R = 0.57; Table 8).

Figure 15 shows the potential ship impact to the total dry deposition of O_3. CMAQ and LOTOS-EUROS are within a similar range, with potential impacts of ships of 5 % to 10 % over water surfaces. The lowest potential impact of -5 % at the main shipping lanes is simulated by CAMx, showing a similar pattern as for the O_3 potential ship impact. Over land areas, ships contribute to dry O_3 deposition from 0.25 % to 2.5 %.

In addition to the impact of O_3 dry deposition on plant stomata, it is important to explain differences in surface O_3 concentration results. The O_3 concentration is sensitive to the deposition velocity (Clifton et al., 2020), which differs among the four CTMs. This can be confirmed by studies comparing deposition schemes, where differences in O_3 concentration between models are caused by the variety of processes (Clifton et al., 2020). In particular, the variability in deposition velocities across models, as discussed in Sect. 3.3.1, is seen as an originator leading to uncertainties in tropospheric O_3 (Wild, 2007). Deposition velocities for the models in the present study (Supplements S19) show lowest velocities for CMAQ. Highest velocities were found for CAMx over land areas. The deposition velocities go along with the annual dry deposition, with high velocities in areas with high dry deposition.

A model comparison study with 15 models by Hardacre et al. (2015) found the greatest differences in total O_3 dry deposition occurring in areas where deposition velocities and O_3 concentrations are highest. Additionally, soil moisture has an important impact on O_3 deposition and concentration. An evaluation study within the CHIMERE model found that especially in southern Europe, where soil is close to the wilting point during summer and affects stomatal opening, O_3 dry deposition declines (Anav et al., 2018). This in turn affects the concentration of gases in the lower atmosphere and thus has an impact on O_3 concentrations.

Table 8: Correlation between models for the whole domain (all grid cells) based on daily data for O_3 total dry deposition.

all	CAMx	CHIMERE	CMAQ	LOTOS-EUROS
LOTOS-EUROS	0.14	0.42	0.20	-
CMAQ	0.26	0.27	-	
CHIMERE	0.57	-		
CAMx	-			

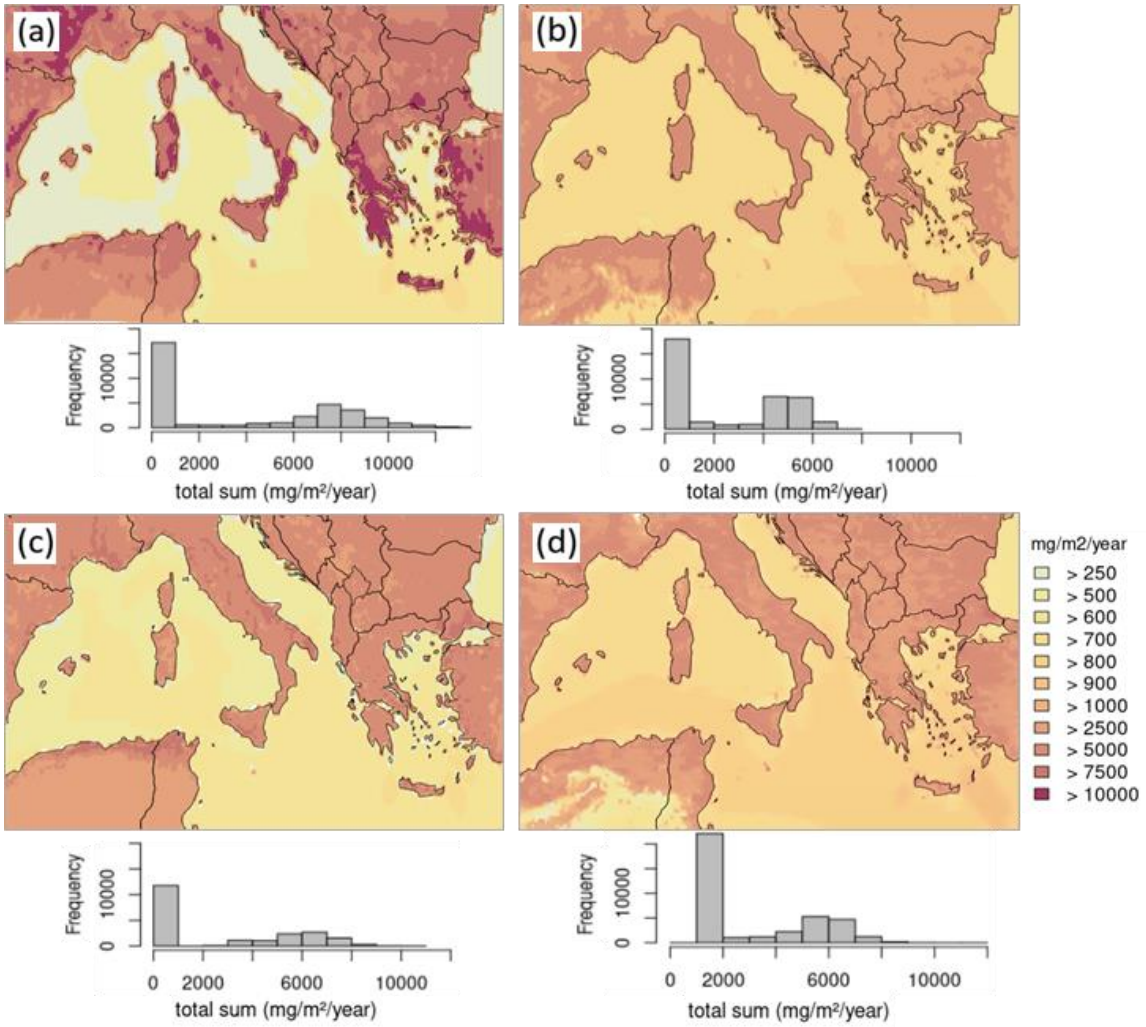

Figure 14: Annual total dry deposition of O_3. (a) = CAMx, (b) = CHIMERE, (c) = CMAQ, (d) = LOTOS-EUROS. Below the domain figure is the respective frequency distribution displayed for the annual mean O_3 dry deposition, referred to the whole model domain.

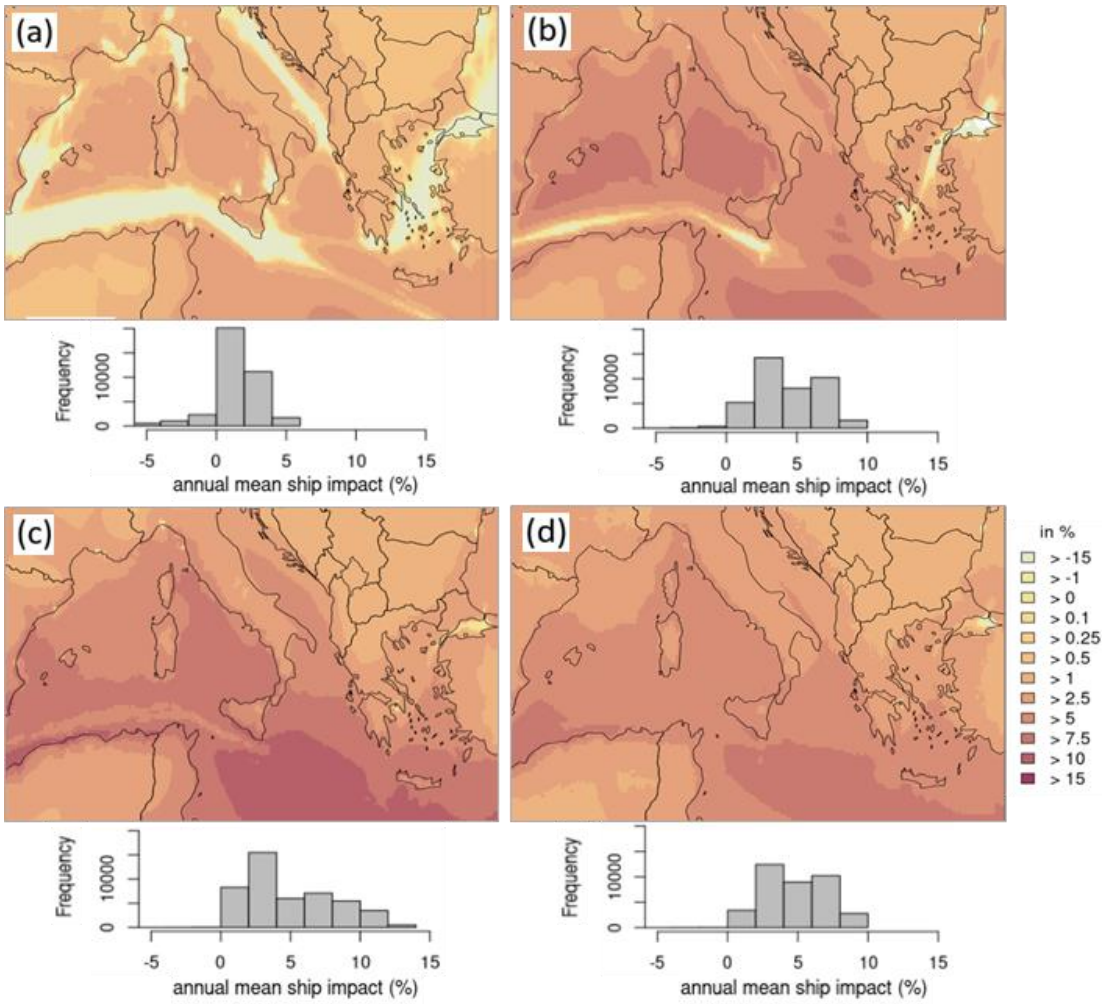

Figure 15: Annual mean dry deposition of O_3 relative ship potential impact. (a) = CAMx, (b) = CHIMERE, (c) = CMAQ, (d) = LOTOS-EUROS. Below the domain figure is the respective frequency distribution displayed for the annual mean O_3 dry deposition ship potential impact, referred to the whole model domain.

4 Summary and Conclusion

The potential impact of ships to air pollution by NO_2 and O_3 the Mediterranean Sea region was simulated with five different regional-scale CTMs (CAMx, CHIMERE, CMAQ, EMEP, LOTOS-EUROS). An evaluation of the results for NO_2 and O_3 concentrations is presented here. By using different CTMs, a more robust estimate of the potential ship impact on atmospheric concentrations and deposition can be obtained compared to single CTM runs.

The emission data, simulated year and domain were the same for all models. The models were run in their standard setup. The CTM simulations were evaluated by comparing the simulated data against the measurements from urban and rural background stations around the Mediterranean Sea.

The focus of the study was the comparison of model simulations concerning the concentration of regulatory pollutants and the calculation of potential ship impacts on air pollution concentrations.

Concerning the results for NO_2, the model performance showed differences in the time series among the models, caused by the large grid size and the differences in meteorology. All five CTMs underestimated the actual measured NO_2 concentration data at most stations, along with results from previous studies (e.g., Karl et al., 2019a; Giordano et al., 2015; Knote et al., 2015). The potential ship impact on the concentration of NO_2 at the measurement stations over land differed among the models. It varied between 1.0 % and 15.3 % at the presented stations. Mean values of the potential impacts of ships on NO_2 at several stations in one area, as shown in the supplements Figures S3-S10, display values up to 48.1 %. This was found in the eastern part of the domain (Figure S7), where the main shipping routes are close to the shore. Previous studies regarding the North and Baltic Seas found similar results because shipping lanes are located closer to the shore and have a higher potential impact on the total NO_2 concentration in coastal regions (Matthias et al., 2010; Karl et al., 2019a). Nevertheless, over water, the model results in the present study display a potential ship impact > 85 % at the main shipping routes. High values are also expected for the African coast since the main shipping route is close, but all measurement stations considered here are in continental Europe; no measurements were available for Northern Africa.

The potential ship impact was similar to the annual mean concentration of NO_2. In both cases, CAMx and CHIMERE displayed the highest annual mean concentration and highest relative potential ship impact. CMAQ, EMEP and LOTOS-EUROS simulated values within one range, which could be confirmed by similarities in the respective frequency distributions.

A relatively good model performance for O_3 was shown by all five CTMs, but the simulations differed in spatial distribution and potential ship impact over water. An overestimation of simulated O_3 concentrations was found at almost all stations. The overestimation of actual measured O_3 by the models agrees with results found in other studies (Appel et al., 2017; Im et al., 2015a, b). Although boxplots for annual mean values of O_3 vary, for relative potential ship impact they show that CHIMERE, CMAQ, EMEP and LOTOS-EUROS are within the same range. The relative potential impact of ships to total O_3 decreases to -20 % in areas with high NO_2 concentrations in all model outputs, but mostly for CAMx. Diurnal cycles did not reveal differences in O_3 depletion over water and land among the models.

The focus of the second part of the present study was dry deposition of NO_2 and O_3. The motivation to examine the dry deposition of NO_2 and O_3 more closely was to potentially explain the model differences found for O_3 and NO_2. Investigations of dry deposition are crucial to explain the conservation of mass and fate of these substances A connection can be seen between a high concentration and low deposition when the deposition velocity is low. This indicates that the substance stays longer in the atmosphere (i.e. CHIMERE). On the other hand, if the deposition rate and deposition are high, the concentration is lower (i.e. LOTOS-EUROS).

Regarding NO_2 dry deposition and the potential ship impact, CAMx showed the highest values. CMAQ displayed the lowest values for NO_2 dry deposition. Along the shoreline, CMAQ and LOTOS-EUROS reveal a potential ship impact between 10 % and 25 %; CAMx and CHIMERE expect a potential ship impact to total annual NO_2 dry deposition of 25 % to 75 %, in some regions also along the coast. These differences are caused by mechanisms to calculate dry deposition velocities, which are unique for each model, as well as differing inputs, such as land use data (Wichink Kruit et al. 2014; Vivanco et al. 2018). The deposition velocities have shown that highest annual mean NO_2 dry deposition were found for CAMx and LOTOS-EUROS, which also had highest deposition velocities.

The potential ship impact on the total dry deposition of O_3 displays the highest impact with values between 75 % and 85 % simulated with CHIMERE. CMAQ and LOTOS-EUROS are within a similar range, with potential ship impacts mainly 5 % to 10 % over water areas. The lowest potential impact of -5 % at main shipping lanes was simulated by CAMx. The correlation of the annual total deposition of O_3 dry deposition was highest for CHIMERE and CAMx. Nevertheless, low to medium correlation was found for all other models. The deposition velocities for O_3 dry deposition has shown a similar pattern as for NO_2: highest velocities were simulated by CAMx and LOTOS-EUROS.

In general, more deviations between the dry deposition model results were found compared to the modelled simulations of the air concentration of pollutants. This is because NO_2 and O_3 in the atmosphere are formed more or less “directly” from the emission data, but dry deposition differs because there are other, model-specific mechanisms behind it.

Overall, in the present study the models were run in their standard setup; a complete harmonization was not the goal. Nevertheless, emissions were harmonized to exclude the source of uncertainty coming from the emission input dataset. This was done to shed light on what other factors except the emission data lead to differences between individual model results.

Furthermore, possible limitations, over- and underestimations of model outputs were pointed out with this intercomparison. Large grid sizes can cause errors insofar as in simulations the land areas are not seen as such but as water areas and vice versa. This is especially problematic when having measurement stations located close to the sea. NO_2 simulations regarding the relative potential ship impact differed more among models compared to the O_3 simulations. Limitations were traced back to the large grid sizes. In addition, model-specific chemistry mechanisms lead to differences in simulated concentrations.

A more reliable estimate of potential ship impacts on the atmospheric concentration as well as deposition can be achieved through an ensemble mean with standard deviations based on different model results. Previous studies have shown that using only one chemistry transport model leads to statistical bias, underestimations of models uncertainties and overconfidence of

results (e.g. Solazzo et al., 2013; Riccio et al., 2012; Solazzo et al., 2018), indicating that a model ensemble should be aimed at. This is of importance, especially regarding the policy point of the study: If model simulations should help in decisions for regulations regarding shipping, the uncertainty of single models should be considered. In the present study, the focus was laid on shipping emissions and their impact NO_2 and O_3 concentrations. It was found that the shipping impact in manycoastal areas of the Mediterranean Sea is smaller compared to the shipping impact in the North and Baltic Sea. This is because the most intensively used shipping lanes are typically further from the coast.

In an additional investigation of potential ship contribution impacts to air pollution, aerosol particles and wet deposition need to be considered, which is the next step in the current intercomparison study. The aerosol formation mechanisms differ among the CTMs; therefore, a detailed investigation of $PM_{2.5}$ and its chemical composition is necessary and will be part of further investigations in the SCIPPER project. Another open question that future studies might answer is the comparison of vertical structures pollution transport. The present study considered the lowest simulated layer, but also mixing of pollutants to higher layers can deliver explanations for differences in lowest layer concentrations.

Acknowledgement

This was work supported by SCIPPER project, which has received funding from the European Union's Horizon 2020 research and innovation programme under grant agreement Nr.814893.

The computations for the regional modeling using the EMEP-model was enabled by resources provided by the Swedish National Infrastructure for Computing (SNIC), partially funded by the Swedish Research Council through grant agreement no. 2018-05973.

References

Agrawal, H., Welch, W. A., Henningsen, S., Miller, J. W., and Cocker, D. R.: Emissions from main propulsion engine on container ship at sea, 35, https://doi.org/10.1029/2009JD013346, 2010.

Agrawal, H., Welch, W. A., Miller, J. W., and Cockert, D. R.: Emission measurements from a crude oil tanker at sea, 19, https://doi.org/10.1021/es703102y, 2008.

Aksoyoglu, S., Baltensperger, U., and Prévôt, A. S. H.: Contribution of ship emissions to the concentration and deposition of air pollutants in Europe, 4, https://doi.org/10.5194/acp-16-1895-2016, 2016.Anav, A., Proietti, C., Menut, L., Carnicelli, S., Marco, A. de, and Paoletti, E.: Sensitivity of stomatal conductance to soil moisture: Implications for tropospheric ozone, 8, https://doi.org/10.5194/acp-18-5747-2018, 2018.

Appel, K. W., Napelenok, S. L., Foley, K. M., Pye, H. O. T., Hogrefe, C., Luecken, D. J., Bash, J. O., Roselle, S. J., Pleim, J. E., Foroutan, H., Hutzell, W. T., Pouliot, G. A., Sarwar, G., Fahey, K. M., Gantt, B., Gilliam, R. C., Heath, N. K., Kang, D., Mathur, R., Schwede, D. B., Spero, T. L., Wong, D. C., and Young, J. O.: Description and evaluation of the Community Multiscale Air Quality (CMAQ) modeling system version 5.1, 4, https://doi.org/10.5194/gmd-10-1703-2017, 2017.

Astitha, M., Lelieveld, J., Abdel Kader, M., Pozzer, A., and Meij, A. de: Parameterization of dust emissions in the global atmospheric chemistry-climate model EMAC: impact of nudging and soil properties, 22, https://doi.org/10.5194/acp-12-11057-2012, 2012.

Aulinger, A., Matthias, V., Zeretzke, M., Bieser, J., Quante, M., and Backes, A.: The impact of shipping emissions on air pollution in the greater North Sea region – Part 1: Current emissions and concentrations, 2, https://doi.org/10.5194/acp-16-739-2016, 2016.

Baldasano, J. M., Pay, M. T., Jorba, O., Gassó, S., and Jiménez-Guerrero, P.: An annual assessment of air quality with the CALIOPE modeling system over Spain, 11, https://doi.org/10.1016/j.scitotenv.2011.01.041, 2011.

Banzhaf, S., Schaap, M., Kerschbaumer, A., Reimer, E., Stern, R., van der Swaluw, E., and Builtjes, P.: Implementation and evaluation of pH-dependent cloud chemistry and wet deposition in the chemical transport model REM-Calgrid, 17, https://doi.org/10.1016/j.atmosenv.2011.10.069, 2012.

Barregard, L., Molnàr, P., Jonson, J. E., and Stockfelt, L.: Impact on Population Health of Baltic Shipping Emissions, 11, https://doi.org/10.3390/ijerph16111954, 2019.

Beltman, J. B., Hendriks, C., Tum, M., and Schaap, M.: The impact of large scale biomass production on ozone air pollution in Europe, Atmos. Environ., 71, 352–363, https://doi.org/10.1016/j.atmosenv.2013.02.019, 2013.

Bergström, R., van der Denier Gon, H. A. C., Prévôt, A. S. H., Yttri, K. E., and Simpson, D.: Modelling of organic aerosols over Europe (2002–2007) using a volatility basis set (VBS) framework: application of different assumptions regarding the formation of secondary organic aerosol, 18, https://doi.org/10.5194/acp-12-8499-2012, 2012.

Bessagnet, B., Pirovano, G., Mircea, M., Cuvelier, C., Aulinger, A., Calori, G., Ciarelli, G., Manders, A., Stern, R., Tsyro, S., García Vivanco, M., Thunis, P., Pay, M.-T., Colette, A., Couvidat, F., Meleux, F., Rouïl, L., Ung, A., Aksoyoglu, S., Baldasano, J. M., Bieser, J., Briganti, G., Cappelletti, A., D'Isidoro, M., Finardi, S., Kranenburg, R., Silibello, C., Carnevale, C., Aas, W., Dupont, J.-C., Fagerli, H., Gonzalez, L., Menut, L., Prévôt, A. S. H., Roberts, P., and White, L.: Presentation of the EURODELTA III intercomparison exercise – evaluation of the chemistry transport models' performance on criteria pollutants and joint analysis with meteorology, 19, https://doi.org/10.5194/acp-16-12667-2016, 2016.

Bieser, J., Aulinger, A., Matthias, V., Quante, M., and Builtjes, P.: SMOKE for Europe – adaptation, modification and evaluation of a comprehensive emission model for Europe, 1, https://doi.org/10.5194/gmd-4-47-2011, 2011a.

Bieser, J., Aulinger, A., Matthias, V., Quante, M., and van der Denier Gon, H. A. C.: Vertical emission profiles for Europe based on plume rise calculations, 10, https://doi.org/10.1016/j.envpol.2011.04.030, 2011b.

Binkowski, F. S. and Shankar, U.: The Regional Particulate Matter Model: 1. Model description and preliminary results, 12, https://doi.org/10.1029/95JD02093, 1995.

Bobbink, R. and Hettelingh, J.-P.: Review and revision of empirical critical loads and dose-response relationships, 2011.

Brandt, J., Silver, J. D., Christensen, J. H., Andersen, M. S., Bønløkke, J. H., Sigsgaard, T., Geels, C., Gross, A., Hansen, A. B., Hansen, K. M., Hedegaard, G. B., Kaas, E., and Frohn, L. M.: Contribution from the ten major emission sectors in Europe and Denmark to the health-cost externalities of air pollution using the EVA model system – an integrated modelling approach, 15, https://doi.org/10.5194/acp-13-7725-2013, 2013.

Byun, D. and Schere, K. L.: Review of the Governing Equations, Computational Algorithms, and Other Components of the Models-3 Community Multiscale Air Quality (CMAQ) Modeling System, 2, https://doi.org/10.1115/1.2128636, 2006.

Carlton, A. G., Bhave, P. V., Napelenok, S. L., Edney, E. O., Sarwar, G., Pinder, R. W., Pouliot, G. A., and Houyoux, M.: Model representation of secondary organic aerosol in CMAQv4.7, 22, https://doi.org/10.1021/es100636q, 2010.

Celik, S., Drewnick, F., Fachinger, F., Brooks, J., Darbyshire, E., Coe, H., Paris, J.-D., Eger, P. G., Schuladen, J., Tadic, I., Friedrich, N., Dienhart, D., Hottmann, B., Fischer, H., Crowley, J. N., Harder, H., and Borrmann, S.: Influence of vessel characteristics and atmospheric processes on the gas and particle phase of ship emission plumes: In situ measurements in the Mediterranean Sea and around the Arabian Peninsula, 8, https://doi.org/10.5194/acp-20-4713-2020.

Clapp, L. J. and Jenkin, M. E.: Analysis of the relationship between ambient levels of O3, NO2 and NO as a function of NOx in the UK, 2001.

Clifton, O. E., Fiore, A. M., Massman, W. J., Baublitz, C. B., Coyle, M., Emberson, L., Fares, S., Farmer, D. K., Gentine, P., Gerosa, G., Guenther, A. B., Helmig, D., Lombardozzi, D. L., Munger, J. W., Patton, E. G., Pusede, S. E., Schwede, D. B., Silva, S. J., Sörgel, M., Steiner, A. L., and Tai, A. P. K.: Dry Deposition of Ozone over Land: Processes, Measurement, and Modeling, 1, https://doi.org/10.1029/2019RG000670, 2020.

Cofala., J., Amann, M., Borken-Kleefeld, J., Gomez-Sanabria, A., Heyes, C., Kiesewetter, G., Sander, R., Schoepp, W., Holland, M., Fagerli, H., and Nyiri, A.: Final Report. The potential for cost-effective air emission reductions from international shipping through designation of further Emission Control Areas in EU waters with focus on the Mediterranean Sea, 2018.

Colette, A., Andersson, C., Manders, A., Mar, K., Mircea, M., Pay, M.-T., Raffort, V., Tsyro, S., Cuvelier, C., Adani, M., Bessagnet, B., Bergström, R., Briganti, G., Butler, T., Cappelletti, A., Couvidat, F., D'Isidoro, M., Doumbia, T., Fagerli, H., Granier, C., Heyes, C., Klimont, Z., Ojha, N., Otero, N., Schaap, M., Sindelarova, K., Stegehuis, A. I., Roustan, Y., Vautard, R., van Meijgaard, E., Vivanco, M. G., and Wind, P.: EURODELTA-Trends, a multi-model experiment of air quality hindcast in Europe over 1990–2010, 9, https://doi.org/10.5194/gmd-10-3255-2017, 2017.

Contini, D., Merico, E.: Recent Advances in Studying Air Quality and Health Effects of Shipping Emissions. Atmosphere, 12, 92. https://doi.org/10.3390/atmos12010092, 2021.

Corbett, J. J. and Fischbeck, P.: Emissions from ships, Science 278 (5339). 823- 824, 1997.

Corbett, J. J., Fischbeck, P., and Pandis, S.: Global nitrogen and sulfur inventories for oceangoing ships, Journal of Geophysical Research-Atmospheres 104 (3). 3457-3470, 1999.

Doche, C., Dufour, G., Foret, G., Eremenko, M., Cuesta, J., Beekmann, M., and Kalabokas, P.: Summertime tropospheric-ozone variability over the Mediterranean basin observed with IASI, 19, https://doi.org/10.5194/acp-14-10589-2014, 2014.

Donahue, N. M., Robinson, A. L., and Pandis, S. N.: Atmospheric organic particulate matter: From smoke to secondary organic aerosol, 1, https://doi.org/10.1016/j.atmosenv.2008.09.055, 2009.

Donateo, A., Gregoris, E., Gambaro, A., Merico, E., Giua, R., Nocioni, A., and Contini, D.: Contribution of harbour activities and ship traffic to PM2.5, particle number concentrations and PAHs in a port city of the Mediterranean Sea (Italy), 15, https://doi.org/10.1007/s11356-014-2849-0, 2014.

Emerson, E. W., Hodshire, A. L., DeBolt, H. M., Bilsback, K. R., Pierce, J. R., McMeeking, G. R., and Farmer, D. K.: Revisiting particle dry deposition and its role in radiative effect estimates, 42, https://doi.org/10.1073/pnas.2014761117, 2020.

Endresen, Ø., Sørgård, E., Sundet, J. K., Dalsøren, S. B., Isaksen, I. S., Berglen, T. F., and Gravir, G.: Emission from international sea transportation and environmental impact, D17, https://doi.org/10.1029/2002JD002898, 2003.

EPA: Health Effects of Ozone Pollution, 2021.

Erisman, J. W., van Pul, A., and Wyers, P.: Parametrization of surface resistance for the quantification of atmospheric deposition of acidifying pollutants and ozone, 16, https://doi.org/10.1016/1352-2310(94)90433-2, 1994.

Eurostat Press Office: World Maritime Day. Half of EU trade in goods is carried by sea, 2016.

Eyring, V., Isaksen, I. S.A., Berntsen, T., Collins, W. J., Corbett, J. J., Endresen, O., Grainger, R. G., Moldanova, J., Schlager, H., and Stevenson, D. S.: Transport impacts on atmosphere and climate: Shipping, 37, https://doi.org/10.1016/j.atmosenv.2009.04.059, 2010.

Fountoukis, C. and Nenes, A.: ISORROPIA II: A computationally efficient thermodynamic equilibrium model for K+–Ca2+–Mg2+–NH4+–Na+–SO42−–NO3−–Cl−–H2O aerosols, 17, https://doi.org/10.5194/acp-7-4639-2007, 2007.

Friedrich, N., Eger, P., Shenolikar, J., Sobanski, N., Schuladen, J., Dienhart, D., Hottmann, B., Tadic, I., Fischer, H., Martinez, M., Rohloff, R., Tauer, S., Harder, H., Pfannerstill, E. Y., Wang, N., Williams, J., Brooks, J., Drewnick, F., Su, H., Li, G., Cheng, Y., Lelieveld, J., and Crowley, J. N.: Reactive nitrogen around the Arabian Peninsula and in the Mediterranean Sea during the 2017 AQABA ship campaign, 10, https://doi.org/10.5194/acp-21-7473-2021, 2021.

Galmarini, S., Makar, P., Clifton, O. E., Hogrefe, C., Bash, J. O., Bellasio, R., Bianconi, R., Bieser, J., Butler, T., Ducker, J., Flemming, J., Hodzic, A., Holmes, C. D., Kioutsioukis, I., Kranenburg, R., Lupascu, A., Perez-Camanyo, J. L., Pleim, J., Ryu, Y.-H., Jose, R. S., Schwede, D., Silva, S., and Wolke, R.: Technical note: AQMEII4 Activity 1: evaluation of wet and dry deposition schemes as an integral part of regional-scale air quality models, 20, https://doi.org/10.5194/acp-21-15663-2021, 2021.

Ginoux, P., Chin, M., Tegen, I., Prospero, J. M., Holben, B., Dubovik, O., and Lin, S.-J.: Sources and distributions of dust aerosols simulated with the GOCART model, D17, https://doi.org/10.1029/2000JD000053, 2001.

Giordano, L., Brunner, D., Flemming, J., Hogrefe, C., Im, U., Bianconi, R., Badia, A., Balzarini, A., Baró, R., Chemel, C., Curci, G., Forkel, R., Jiménez-Guerrero, P., Hirtl, M., Hodzic, A., Honzak, L., Jorba, O., Knote, C., Kuenen, J.J.P., Makar, P. A., Manders-Groot, A., Neal, L., Pérez, J. L., Pirovano, G., Pouliot, G., San José, R., Savage, N., Schröder, W., Sokhi, R. S., Syrakov, D., Torian, A., Tuccella, P., Werhahn, J., Wolke, R., Yahya, K., Žabkar, R., Zhang, Y., and Galmarini, S.: Assessment of the MACC reanalysis and its influence as chemical boundary conditions for regional air quality modeling in AQMEII-2, 1, https://doi.org/10.1016/j.atmosenv.2015.02.034, 2015.

Gong, S. L.: A parameterization of sea-salt aerosol source function for sub- and super-micron particles, 4, https://doi.org/10.1029/2003gb002079, 2003.

Granier, C., Darras, S., van der Denier Gon, H., Doubalova, J., Elguindi, N., Galle, B., Gauss, M., Guevara, M., Jalkanen, J.-P., Kuenen, J., Liousse, C., Quack, B., Simpson, D., and Sindelarova, K.: The Copernicus Atmosphere Monitoring Service global and regional emissions: (April 2019 version), Copernicus Atmosphere Monitoring Service (CAMS) report, https://doi.org/10.24380/d0bn-kx16, 2019.

Guenther, A., Karl, T., Harley, P., Wiedinmyer, C., Palmer, P. I., and Geron, C.: Estimates of global terrestrial isoprene emissions using MEGAN (Model of Emissions of Gases and Aerosols from Nature), 11, 30 pp., https://doi.org/10.5194/acp-6-3181-2006, 2006.

Guenther, A. B., Jiang, X., Heald, C. L., Sakulyanontvittaya, T., Duhl, T., Emmons, L. K., and Wang, X.: The Model of Emissions of Gases and Aerosols from Nature version 2.1 (MEGAN2.1): An extended and updated framework for modeling biogenic emissions, 6, 22 pp., https://doi.org/10.5194/gmd-5-1471-2012, 2012.

Hardacre, C., Wild, O., and Emberson, L.: An evaluation of ozone dry deposition in global scale chemistry climate models, 11, https://doi.org/10.5194/acp-15-6419-2015, 2015.

Hicks, B. B., Baldocchi, D. D., Meyers, T. P., Hosker, R. P., and Matt, D. R.: A preliminary multiple resistance routine for deriving dry deposition velocities from measured quantities, 3-4, https://doi.org/10.1007/BF00229675, 1987.

Im, U., Christodoulaki, S., Violaki, K., Zarmpas, P., Kocak, M., Daskalakis, N., Mihalopoulos, N., and Kanakidou, M.: Atmospheric deposition of nitrogen and sulfur over southern Europe with focus on the Mediterranean and the Black Sea, 1, https://doi.org/10.1016/j.atmosenv.2013.09.048, 2013.

Im, U., Bianconi, R., Solazzo, E., Kioutsioukis, I., Badia, A., Balzarini, A., Baró, R., Bellasio, R., Brunner, D., Chemel, C., Curci, G., Flemming, J., Forkel, R., Giordano, L., Jiménez-Guerrero, P., Hirtl, M., Hodzic, A., Honzak, L., Jorba, O., Knote, C., Kuenen, J. J.P., Makar, P. A., Manders-Groot, A., Neal, L., Pérez, J. L., Pirovano, G., Pouliot, G., San Jose, R., Savage, N., Schroder, W., Sokhi, R. S., Syrakov, D., Torian, A., Tuccella, P., Werhahn, J., Wolke, R., Yahya, K., Zabkar, R., Zhang, Y., Zhang, J., Hogrefe, C., and Galmarini, S.: Evaluation of operational on-line-coupled regional air quality models over Europe and North America in the context of AQMEII phase 2. Part I: Ozone, 4, https://doi.org/10.1016/j.atmosenv.2014.09.042, 2015a.

Im, U., Bianconi, R., Solazzo, E., Kioutsioukis, I., Badia, A., Balzarini, A., Baró, R., Bellasio, R., Brunner, D., Chemel, C., Curci, G., van der Denier Gon, H., Flemming, J., Forkel, R., Giordano, L., Jiménez-Guerrero, P., Hirtl, M., Hodzic, A., Honzak, L., Jorba, O., Knote, C., Makar, P. A., Manders-Groot, A., Neal, L., Pérez, J. L., Pirovano, G., Pouliot, G., San Jose, R., Savage, N., Schroder, W., Sokhi, R. S., Syrakov, D., Torian, A., Tuccella, P., Wang, K., Werhahn, J., Wolke, R., Zabkar, R., Zhang, Y., Zhang, J., Hogrefe, C., and Galmarini, S.: Evaluation of operational online-coupled regional air quality models over Europe and North America in the context of AQMEII phase 2. Part II: Particulate matter, 17, https://doi.org/10.1016/j.atmosenv.2014.08.072, 2015b.

Inness, A., Ades, M., Agustí-Panareda, A., Barré, J., Benedictow, A., Blechschmidt, A.-M., Dominguez, J. J., Engelen, R., Eskes, H., Flemming, J., Huijnen, V., Jones, L., Kipling, Z., Massart, S., Parrington, M., Peuch, V.-H., Razinger, M., Remy,

S., Schulz, M., and Suttie, M.: The CAMS reanalysis of atmospheric composition, 6, https://doi.org/10.5194/acp-19-3515-2019, 2019.

Jägerbrand, A. K., Brutemark, A., Barthel Svedén, J., and Gren, I.-M.: A review on the environmental impacts of shipping on aquatic and nearshore ecosystems, https://doi.org/10.1016/j.scitotenv.2019.133637, 2019.

Jalkanen, J.-P., Johansson, L., Kukkonen, J., Brink, A., Kalli, J., and Stipa, T.: Extension of an assessment model of ship traffic exhaust emissions for particulate matter and carbon monoxide, 5, 19 pp., https://doi.org/10.5194/acp-12-2641-2012, 2012.

Jalkanen, J.-P., Johansson, L., and Kukkonen, J.: A comprehensive inventory of ship traffic exhaust emissions in the European sea areas in 2011, 1, https://doi.org/10.5194/acp-16-71-2016, 2016.

Jalkanen, J.-P., Brink, A., Kalli, J., Pettersson, H., Kukkonen, J., and Stipa, T.: A modelling system for the exhaust emissions of marine traffic and its application in the Baltic Sea area, 23, https://doi.org/10.5194/acp-9-9209-2009, 2009.

Johansson, L., Jalkanen, J.-P., Kalli, J., and Kukkonen, J.: The evolution of shipping emissions and the costs of regulation changes in the northern EU area, 22, https://doi.org/10.5194/acp-13-11375-2013, 2013.

Johansson, L., Jalkanen, J.-P., and Kukkonen, J.: Global assessment of shipping emissions in 2015 on a high spatial and temporal resolution, 2, https://doi.org/10.1016/j.atmosenv.2017.08.042, 2017.

Jonson, J. E., Jalkanen, J. P., Johansson, L., Gauss, M., and van der Denier Gon, H. A. C.: Model calculations of the effects of present and future emissions of air pollutants from shipping in the Baltic Sea and the North Sea, 2, https://doi.org/10.5194/acp-15-783-2015, 2015.

Jutterström, S., Moldan, F., Moldanová, J., Karl, M., Matthias, V., and Posch, M.: The impact of nitrogen and sulfur emissions from shipping on the exceedance of critical loads in the Baltic Sea region, Atmos. Chem. Phys., 21, 15827–15845, https://doi.org/10.5194/acp-21-15827-2021, 2021.

Karl, M., Jonson, J. E., Uppstu, A., Aulinger, A., Prank, M., Jalkanen, J.-P., Johansson, L., Quante, M., and Matthias, V.: Effects of ship emissions on air quality in the Baltic Sea region simulated with three different chemistry transport models, https://doi.org/10.5194/acp-2018-1317, 2019a.

Karl, M., Bieser, J., Geyer, B., Matthias, V., Jalkanen, J.-P., Johansson, L., and Fridell, E.: Impact of a nitrogen emission control area (NECA) on the future air quality and nitrogen deposition to seawater in the Baltic Sea region, 3, https://doi.org/10.5194/acp-19-1721-2019, 2019b.

Kelly, J. T., Bhave, P. V., Nolte, C. G., Shankar, U., and Foley, K. M.: Simulating emission and chemical evolution of coarse sea-salt particles in the Community Multiscale Air Quality (CMAQ) model, 1, https://doi.org/10.5194/gmd-3-257-2010, 2010.

Klingmüller, K., Metzger, S., Abdelkader, M., Karydis, V. A., Stenchikov, G. L., Pozzer, A., and Lelieveld, J.: Revised mineral dust emissions in the atmospheric chemistry-climate model EMAC (based on MESSy 2.52), https://doi.org/10.5194/gmd-2017-160, 2017.

Knote, C., Tuccella, P., Curci, G., Emmons, L., Orlando, J. J., Madronich, S., Baró, R., Jiménez-Guerrero, P., Luecken, D., Hogrefe, C., Forkel, R., Werhahn, J., Hirtl, M., Pérez, J. L., San José, R., Giordano, L., Brunner, D., Yahya, K., and Zhang, Y.: Influence of the choice of gas-phase mechanism on predictions of key gaseous pollutants during the AQMEII phase-2 intercomparison, 40, https://doi.org/10.1016/j.atmosenv.2014.11.066, 2015.

Köhler, I., Sausen, R., & Klenner, G.: NOx production from lightning, the impact of NOx emissions from aircraft upon the atmosphere at flight altitudes 8–15 km (AERONOX), edited by U. Schumann, final report to the Comm. of the Eur. Commun., Dtsch. Luft und Raumfahrt, Oberpfaffenhofen, Germany, 1995.

Liu, J. J., Jones, D. B. A., Worden, J. R., Noone, D., Parrington, M., and Kar, J.: Analysis of the summertime buildup of tropospheric ozone abundances over the Middle East and North Africa as observed by the Tropospheric Emission Spectrometer instrument, D5, https://doi.org/10.1029/2008JD010993, 2009.

Manders, A. M. M., Builtjes, P. J. H., Curier, L., van der Denier Gon, H. A. C., Hendriks, C., Jonkers, S., Kranenburg, R., Kuenen, J. J. P., Segers, A. J., Timmermans, R. M. A., Visschedijk, A. J. H., Wichink Kruit, R. J., van Pul, W. A. J., Sauter, F. J., van der Swaluw, E., Swart, D. P. J., Douros, J., Eskes, H., van Meijgaard, E., van Ulft, B., van Velthoven, P., Banzhaf, S., Mues, A. C., Stern, R., Fu, G., Lu, S., Heemink, A., van Velzen, N., and Schaap, M.: Curriculum vitae of the LOTOS–EUROS (v2.0) chemistry transport model, 11, https://doi.org/10.5194/gmd-10-4145-2017, 2017.

Manders-Groot, A., Segers, A., and Jonkers, S.: LOTOS-EUROS v2.0 Reference Guide, 2016.

Marmer, E. and Langmann, B.: Impact of ship emissions on the Mediterranean summertime pollution and climate: A regional model study, 26, https://doi.org/10.1016/j.atmosenv.2005.04.014, 2005.

Mårtensson, E. M., Nilsson, E. D., Leeuw, G. de, Cohen, L. H., and Hansson, H.-C.: Laboratory simulations and parameterization of the primary marine aerosol production, D9, https://doi.org/10.1029/2002JD002263, 2003.

Matthias, V., Bewersdorff, I., Aulinger, A., and Quante, M.: The contribution of ship emissions to air pollution in the North Sea regions, 6, https://doi.org/10.1016/j.envpol.2010.02.013, 2010.

Menut, L., Bessagnet, B., Khvorostyanov, D., Beekmann, M., Blond, N., Colette, A., Coll, I., Curci, G., Foret, G., Hodzic, A., Mailler, S., Meleux, F., Monge, J.-L., Pison, I., Siour, G., Turquety, S., Valari, M., Vautard, R., and Vivanco, M. G.: CHIMERE 2013: A model for regional atmospheric composition modelling, 4, https://doi.org/10.5194/gmd-6-981-2013, 2013.

Merico, E., Donateo, A., Gambaro, A., Cesari, D., Gregoris, E., Barbaro, E., Dinoi, A., Giovanelli, G., Masieri, S., and Contini, D.: Influence of in-port ships emissions to gaseous atmospheric pollutants and to particulate matter of different sizes in a Mediterranean harbour in Italy, 10, https://doi.org/10.1016/j.atmosenv.2016.05.024, 2016.

Merico, E., Gambaro, A., Argiriou, A., Alebic-Juretic, A., Barbaro, E., Cesari, D., Chasapidis, L., Dimopoulos, S., Dinoi, A., Donateo, A., Giannaros, C., Gregoris, E., Karagiannidis, A., Konstandopoulos, A. G., Ivošević, T., Liora, N., Melas, D., Mifka, B., Orlić, I., Poupkou, A., Sarovic, K., Tsakis, A., Giua, R., Pastore, T., Nocioni, A., and Contini, D.: Atmospheric impact of ship traffic in four Adriatic-Ionian port-cities: Comparison and harmonization of different approaches, 11, https://doi.org/10.1016/j.trd.2016.11.016, 2017.

Möller, D.: Luft, https://doi.org/10.1515/9783110200225, 2003.

Mokhtari, M., Gomes, L., Tulet, P., and Rezoug, T.: Importance of the surface size distribution of erodible material: an improve[1]ment on the Dust Entrainment And Deposition (DEAD) Model, Geosci. Model Dev., 5, 581–598, https://doi.org/10.5194/gmd-5- 581-2012, 2012.

Monahan, E. C., Spiel, D. E., and Davidson, K. L.: A Model of Marine Aerosol Generation Via Whitecaps and Wave Disruption, https://doi.org/10.1007/978-94-009-4668-2_16, 1986.

Nenes, A., Pandis, S. N., and Pilinis, C.: ISORROPIA: A New Thermodynamic Equilibrium Model for Multiphase Multicomponent Inorganic Aerosols, 1, https://doi.org/10.1023/A:1009604003981, 1998.

Novak, J. H. and Pierce, T. E.: Natural emissions of oxidant precursors, Water Air Soil Poll., 67, 57–77, https://doi.org/10.1007/BF00480814, 1993.

Nunes, R. A. O., Alvim-Ferraz, M. C. M., Martins, F. G., Calderay-Cayetano, F., Durán-Grados, V., Moreno-Gutiérrez, J., Jalkanen, J.-P., Hannuniemi, H., and Sousa, S. I. V.: Shipping emissions in the Iberian Peninsula and the impacts on air quality, 15, https://doi.org/10.5194/acp-20-9473-2020, 2020.

Ordóñez, C., Richter, A., Steinbacher, M., Zellweger, C., Nüß, H., Burrows, J. P., and Prévôt, A. S. H.: Comparison of 7 years of satellite-borne and ground-based tropospheric NO2 measurements around Milan, Italy, D5, https://doi.org/10.1029/2005JD006305, 2006.

Ovadnevaite, J., Manders, A., Leeuw, G. de, Ceburnis, D., Monahan, C., Partanen, A.-I., Korhonen, H., and O'Dowd, C. D.: A sea spray aerosol flux parameterization encapsulating wave state, 4, https://doi.org/10.5194/acp-14-1837-2014, 2014.

Petrik, R., Geyer, B., and Rockel, B.: On the diurnal cycle and variability of winds in the lower planetary boundary layer: evaluation of regional reanalyses and hindcasts, 1, https://doi.org/10.1080/16000870.2020.1804294, 2021.

Pleim, J. and Ran, L.: Surface Flux Modeling for Air Quality Applications, 3, https://doi.org/10.3390/atmos2030271, 2011.

Pleim, J. E., Xiu, A., Finkelstein, P. L., and Otte, T. L.: A Coupled Land-Surface and Dry Deposition Model and Comparison to Field Measurements of Surface Heat, Moisture, and Ozone Fluxes, 5/6, https://doi.org/10.1023/A:1013123725860, 2001.

Prati, M. V., Costagliola, M. A., Quaranta, F., and Murena, F.: Assessment of ambient air quality in the port of Naples, 8, https://doi.org/10.1080/10962247.2015.1050129, 2015.

Prigent, C., Jiménez, C., and Catherinot, J.: Comparison of satellite microwave backscattering (ASCAT) and visible/near-infrared reflectances (PARASOL) for the estimation of aeolian aerodynamic roughness length in arid and semi-arid regions, https://doi.org/10.5194/amtd-5-2933-2012, 2012.

Pye, H. O. T. and Pouliot, G. A.: Modeling the role of alkanes, polycyclic aromatic hydrocarbons, and their oligomers in secondary organic aerosol formation, 11, 2012.

Ramboll Environment and Health: User's Guide COMPREHENSIVE AIR QUALITY MODEL WITH EXTENSIONS: Version 7.10, 2020.

Reichle, L. J., Cook, R., Yanca, C. A., and Sonntag, D. B.: Development of organic gas exhaust speciation profiles for nonroad spark-ignition and compression-ignition engines and equipment, 10, https://doi.org/10.1080/10962247.2015.1020118, 2015.

Robinson, A. L., Donahue, N. M., Shrivastava, M. K., Weitkamp, E. A., Sage, A. M., Grieshop, A. P., Lane, T. E., Pierce, J. R., and Pandis, S. N.: Rethinking organic aerosols: semivolatile emissions and photochemical aging, 5816, https://doi.org/10.1126/science.1133061, 2007.

Safieddine, S., Boynard, A., Coheur, P.-F., Hurtmans, D., Pfister, G., Quennehen, B., Thomas, J. L., Raut, J.-C., Law, K. S., Klimont, Z., Hadji-Lazaro, J., George, M., and Clerbaux, C.: Summertime tropospheric ozone assessment over the Mediterranean region using the thermal infrared IASI/MetOp sounder and the WRF-Chem model, 18, https://doi.org/10.5194/acp-14-10119-2014, 2014.

Schaap, M., Timmermans, R. M.A., Roemer, M., Boersen, G.A.C., Builtjes, P. J.H., Sauter, F. J., Velders, G. J.M., and Beck, J. P.: The LOTOS EUROS model: Description, validation and latest developments, 2, https://doi.org/10.1504/IJEP.2008.017106, 2008.

Schembari, C., Cavalli, F., Cuccia, E., Hjorth, J., Calzolai, G., Pérez, N., Pey, J., Prati, P., and Raes, F.: Impact of a European directive on ship emissions on air quality in Mediterranean harbours, 3, https://doi.org/10.1016/j.atmosenv.2012.06.047, 2012.

Schober, P., Boer, C., and Schwarte, L. A.: Correlation Coefficients: Appropriate Use and Interpretation, 5, https://doi.org/10.1213/ANE.0000000000002864, 2018.

Schultze, M. and Rockel, B.: Direct and semi-direct effects of aerosol climatologies on long-term climate simulations over Europe, 9-10, https://doi.org/10.1007/s00382-017-3808-5, 2018.

Schulz, M., Textor, C., Kinne, S., Balkanski, Y., Bauer, S., Berntsen, T., Berglen, T., Boucher, O., Dentener, F., Guibert, S., Isaksen, I. S. A., Iversen, T., Koch, D., Kirkevåg, A., Liu, X., Montanaro, V., Myhre, G., Penner, J. E., Pitari, G., Reddy, S., Seland, Ø., Stier, P., and Takemura, T.: Radiative forcing by aerosols as derived from the AeroCom present-day and pre-industrial simulations, 12, https://doi.org/10.5194/acp-6-5225-2006, 2006.

Simpson, D., Benedictow, A., Berge, H., Bergström, R., Emberson, L. D., Fagerli, H., Flechard, C. R., Hayman, G. D., Gauss, M., Jonson, J. E., Jenkin, M. E., Nyíri, A., Richter, C., Semeena, V. S., Tsyro, S., Tuovinen, J.-P., Valdebenito, Á., and Wind, P.: The EMEP MSC-W chemical transport model – technical description, 16, https://doi.org/10.5194/acp-12-7825-2012, 2012.

Simpson, D., Fagerli, H., Jonson, J. E., Tsyro, S., and Wind, P.: Transboundary Acidification, Eutrophication and Ground Level Ozone in Europe. PART I. Unified EMEP Model Description., 2003.

Simpson, D., Bergström, R., Briolat, A., Imhof, H., Johansson, J., Priestley, M., and Valdebenito, A.: GenChem v1.0 – a chemical pre-processing and testing system for atmospheric modelling, 12, https://doi.org/10.5194/gmd-13-6447-2020, 2020.

Sippula, O., Stengel, B., Sklorz, M., Streibel, T., Rabe, R., Orasche, J., Lintelmann, J., Michalke, B., Abbaszade, G., Radischat, C., Gröger, T., Schnelle-Kreis, J., Harndorf, H., and Zimmermann, R.: Particle emissions from a marine engine: chemical composition and aromatic emission profiles under various operating conditions, 19, https://doi.org/10.1021/es502484z, 2014.

Solazzo, E., Riccio, A., van Dingenen, R., Valentini, L., and Galmarini, S.: Evaluation and uncertainty estimation of the impact of air quality modelling on crop yields and premature deaths using a multi-model ensemble, https://doi.org/10.1016/j.scitotenv.2018.03.317, 2018.

Tadic, I., Crowley, J. N., Dienhart, D., Eger, P., Harder, H., Hottmann, B., Martinez, M., Parchatka, U., Paris, J.-D., Pozzer, A., Rohloff, R., Schuladen, J., Shenolikar, J., Tauer, S., Lelieveld, J., and Fischer, H.: Net ozone production and its relationship to nitrogen oxides and volatile organic compounds in the marine boundary layer around the Arabian Peninsula, 11, https://doi.org/10.5194/acp-20-6769-2020, 2020.

Tysro, S. G. and Berge, E.: The Contribution of Ship Emission from the North Sea and the North-eastern Atlantic Ocean to Acidification in Europe, EMEP/MSC-W Note 4/97. EMEP. Meteorol. Synthesizing Centre e West, Norwegian Meteorological Institute, Oslo. Norway, 1997.

van Zanten, M. C., Sauter, F. J., Wichink Kruit, R. J., van Jaarsveld, J. A., and van Pul, W. A. J.: Description of the DEPAC module: Dry deposition modelling with DEPAC_GCN2010, 76 pp., 2010.

Večeřa, Z., Mikuška, P., Smolík, J., Eleftheriadis, K., Bryant, C., Colbeck, I., and Lazaridis, M.: Shipboard Measurements of Nitrogen Dioxide, Nitrous Acid, Nitric Acid and Ozone in the Eastern Mediterranean Sea, 1, https://doi.org/10.1007/s11267-007-9133-y, 2008.

Viana, M., Hammingh, P., Colette, A., Querol, X., Degraeuwe, B., Vlieger, I. d., and van Aardenne, J.: Impact of maritime transport emissions on coastal air quality in Europe, https://doi.org/10.1016/j.atmosenv.2014.03.046, 2014.

Vivanco, M. G., Theobald, M. R., García-Gómez, H., Garrido, J. L., Prank, M., Aas, W., Adani, M., Alyuz, U., Andersson, C., Bellasio, R., Bessagnet, B., Bianconi, R., Bieser, J., Brandt, J., Briganti, G., Cappelletti, A., Curci, G., Christensen, J. H., Colette, A., Couvidat, F., Cuvelier, C., D'Isidoro, M., Flemming, J., Fraser, A., Geels, C., Hansen, K. M., Hogrefe, C., Im, U.,

Jorba, O., Kitwiroon, N., Manders, A., Mircea, M., Otero, N., Pay, M.-T., Pozzoli, L., Solazzo, E., Tsyro, S., Unal, A., Wind, P., and Galmarini, S.: Modeled deposition of nitrogen and sulfur in Europe estimated by 14 air quality model systems: evaluation, effects of changes in emissions and implications for habitat protection, 14, https://doi.org/10.5194/acp-18-10199-2018, 2018.

Wesely, M. L.: Parameterization of surface resistances to gaseous dry deposition in regional-scale numerical models, 6, https://doi.org/10.1016/0004-6981(89)90153-4, 1989.

Whitten, G. Z., Heo, G., Kimura, Y., McDonald-Buller, E., Allen, D. T., Carter, W. P.L., and Yarwood, G.: A new condensed toluene mechanism for Carbon Bond: CB05-TU☆, 40, 12 pp., https://doi.org/10.1016/j.atmosenv.2009.12.029, 2010.

Wichink Kruit, R. J., Schaap, M., Sauter, F. J., van Zanten, M. C., and van Pul, W. A. J.: Modeling the distribution of ammonia across Europe including bi-directional surface-atmosphere exchange, https://doi.org/10.5194/bgd-9-4877-2012, 2012.

Wichink Kruit, R. W., Schaap, M., Segers, A., Heslinga, D., Builtjes, P., Branzhaf, S., and Scheuschner, T.: Modelling and mapping of atmospheric nitrogen and sulphur deposition and critical loads for ecosystem specific assessment of threats to biodiversity in Germany – PINETI (Pollutant INput and EcosysTem Impact) Substudy Report 1., 2014.

Wiedinmyer, C., Akagi, S. K., Yokelson, R. J., Emmons, L. K., Al-Saadi, J. A., Orlando, J. J., and Soja, A. J.: The Fire INventory from NCAR (FINN): A high resolution global model to estimate the emissions from open burning, 3, https://doi.org/10.5194/gmd-4-625-2011, 2011.

Wild, O.: Modelling the global tropospheric ozone budget: Exploring the variability in current models, 10, https://doi.org/10.5194/acp-7-2643-2007, 2007.

Yarwood, G., Rao, S., Yocke, M., and Whitten, G. Z.: Updates to the carbon bond chemical mechanism: CB05. 2005.

van Zanten, M. C., Sauter, F. J., Wichink Kruit, R. J., van Jaarsveld, J. A., and van Pul, W.A.J.: Description of the DEPAC module: Dry deposition modelling with DEPAC_GCN2010, RIVM Report 680180001/2010, 2010.

Zhang, L., Brook, J. R., and Vet, R.: A revised parameterization for gaseous dry deposition in air-quality models, 6, https://doi.org/10.5194/acp-3-2067-2003, 2003.

Appendix

Appendix A: Definitions of NMB, R and RMSE

$$\text{Normalized Mean Bias (NMB)} = \frac{\sum_1^n (M-O)}{\sum_1^n (O)} \quad (1)$$

where *M* and *O* stand for model and observation results, respectively. The time average is indicated over n time intervals (number of observations). The time average is done for one year.

$$\text{Correlation (R)} = \frac{1}{(n-1)} \sum_1^n \left(\left(\frac{O-\overline{O}}{\sigma_o} \right) * \left(\frac{M-\overline{M}}{\sigma_m} \right) \right) \quad (2)$$

$$\text{Root Mean Square Error (RMSE)} = \sqrt{\frac{\sum_1^n (M-O)^2}{n}} \quad (3)$$

RMSE is a measure of accuracy and allows prediction errors of different models to be compared for a particular dataset.

Appendix B:

Table B1: detailed overview of monitoring stations

Name	Code	Country	Latitude	Longitude	Ele-vation	Station Type	Data Points	Measured Pollutants
Vlora	al0204a	Albania	40.40309	19.4862	25	urban background	6850	benzene, CO, NO_2, NO_x, O_3, PM_{10}, $PM_{2.5}$, SO_2
Shkoder	al0206a	Albania	42.3139	19.52342	13	urban background	7536	CO, NO_2, NO_x, O_3, PM_{10}, $PM_{2.5}$, SO_2
Els Torms	es0014r	Spain	41.39389	0.73472	470	rural background	8549	NO, NO_2, NO_x, O_3, SO_2
Vila-seca (RENFE)	es1117a	Spain	41.11209	1.151824	41	suburban background	8594	NO, NO_2, NO_x
Sant Celoni (Carles Damm)	es1275a	Spain	41.68905	2.495747	145	suburban background	7180	NO, NO_x, NO_2, SO_2
Barcelona (Ciutadella)	es1679a	Spain	41.38641	2.187417	7	urban background	8565	NO, NO_2, NO_x
Mataró (passeig dels Molins)	es1816a	Spain	41.54716	2.443254	40	urban background	8484	NO, NO_x, NO_2, O_3, CO
Barcelona (Palau Reial)	es1992a	Spain	41.38748	2.11515	81	urban background	8393	NO, NO_2, NO_x, SO_2, CO
Marseille 5 Avenues	fr03043	France	43.30607	5.395794	73	urban background	8585	NO_2, O_3, PM_{10}, $PM_{2.5}$, SO_2
Esterel	fr03070	France	43.43786	6.768366	5	suburban background	1820	NO_2, O_3
Agathois-piscénois	fr08022	France	43.28776	3.504831	20	suburban background	8382	NO_2, O_3
Gauzy	fr08614	France	43.8344	4.374219	40	urban background	8406	NO_2, O_3, PM_{10}, $PM_{2.5}$
Rigaud	fr08713	France	42.68402	2.903453	50	urban background	8419	NO_2, PM_{10}

Cannes Broussilles	fr24009	France	43.5625	7.007222	71	urban background	8587	NO_2, O_3, PM_{10}, $PM_{2.5}$
Manosque	fr24018	France	43.83527	5.785831	385	urban background	8517	NO_2, O_3, PM_{10}, $PM_{2.5}$
Nice Arson	fr24036	France	43.70207	7.286264	11	urban background	8701	NO_2, O_3, PM_{10}, $PM_{2.5}$
Ajaccio Sposata	fr41007	France	41.94923	8.757586	60	suburban background	8497	NO_2, O_3
Bastia Montesoro	fr41017	France	42.67134	9.434644	47	rural background	8626	NO_2, O_3, $PM_{2.5}$
Lykovrysi	gr0035a	Greece	38.06963	23.77689	210	suburban background	6719	NO_2, NO_2, O_3
Neochorouda	gr0045a	Greece	40.73984	22.87623	229	suburban background	8725	NO_2, NO, O_3
Finokalia	gr0002r	Greece	35.315871	25.666216	250	rural background	6825	PM_{10}, O_3
NA	hr0025a	Croatia	44.86247	13.81686	0	suburban background	8293	NO_2, NO_x, O_3
Melilli	it0611a	Italy	37.18237	15.12883	300	urban background	7964	NO_2, O_3, SO_2
Priolo	it0614a	Italy	37.15612	15.19087	35	urban background	7902	NO_2, benzene, SO_2
SR - Via Gela	it0620a	Italy	37.10247	15.26564	60	suburban background	6958	NO_2, O_3, SO_2
Gela-Enimed	it0815a	Italy	37.06222	14.28422	13	suburban background	8052	NO_2, SO_2, benzene
Aprilia	it0865a	Italy	41.59528	12.65361	83	urban background	8169	NO_2
Leonessa	it0989a	Italy	42.5725	12.96194	948	urban background	8207	NO_2, O_3
Gherardi	it1179a	Italy	44.83972	11.96111	-2	rural background	8269	NO_x, NO_2, O_3

Adria	it1213a	Italy	45.04667	12.06194	4	urban background	8306	NO_2, NO_x, O_3
Cennm1	it1375a	Italy	39.44361	9.015278	124	rural background	7595	NO_2, SO_2
Teatro d'Annunzio	it1423a	Italy	42.45639	14.23472	4	urban background	8135	NO_2, O_3, PM_{10}, $PM_{2.5}$, SO_2, benzene, CO
Cenps7	it1576a	Italy	39.20333	8.386111	25	suburban background	7968	CO, NO_2, SO_2
Taranto San Vito	it1610a	Italy	40.42333	17.22528	10	urban background	7871	NO_2
Lecce - S.M. Cerrate	it1665a	Italy	40.45889	18.11611	10	rural background	7290	NO_2, O_3
Brindisi Via Magellano	it1702a	Italy	40.65083	17.94361	10	suburban background	7904	NO_2, PM_{10}
Genga - Parco Gola della Rossa	it1773a	Italy	43.46806	12.95222	550	rural background	5310	NO_2, O_3, PM_{10}, $PM_{2.5}$, SO_2, benzene, CO
Civitanova Ippodromo S. Marone	it1796a	Italy	43.33556	13.67472	110	rural background	6699	NO_2, NO_x, O_3, PM_{10}, $PM_{2.5}$, benzene
Guardiaregia	it1806a	Italy	41.41889	14.52556	884	rural background	7892	NO_2, NO_x, O_3, SO_2
Ancona Cittadella	it1827a	Italy	43.61167	13.50861	100	urban background	5985	NO_2, O_3, PM_{10}, $PM_{2.5}$, benzene, CO, SO_2
Schivenoglia	it1865a	Italy	44.99694	11.07083	16	rural background	8325	NO_2, NO_x, O_3, SO_2, benzene
Trapani	it1898a	Italy	38.01237	12.54689	40	urban background	7396	NO_2, O_3, benzene, CO
San Rocco	it1914a	Italy	44.87306	10.66389	22	rural background	8398	NO_2, NO_x, O_3
Locri	it1940a	Italy	38.22976	16.25518	11	urban background	8509	NO_2, O_3, SO_2, benzene, CO

GR - Maremma	it1942a	Italy	42.67056	11.09417	40	rural background	7784	NO_2, O_3
Censa3	it1947a	Italy	39.06667	9.008889	56	urban background	8169	NO_2, SO_2, benzene
Milazzo - Termica	it1997a	Italy	38.19061	15.24911	28	suburban background	8329	NO_2, O_3, CO, benzene
Stadio Casardi	it2003a	Italy	41.31667	16.28611	15	urban background	8391	NO_2, O_3, benzene
Cenqu1	it2040a	Italy	39.23278	9.188056	8	urban background	8181	NO_2, O_3, SO_2, benzene
Carbonara	it2051a	Italy	41.07694	16.86583	130	suburban background	7505	NO_2, PM_{10}
Ceglie Messapica	it2148a	Italy	40.64917	17.5125	100	suburban background	8393	NO_2, PM_{10}, $PM_{2.5}$, SO_2, CO, benzene
LI - Piombino-Parco-VIII-Marzo	it2154a	Italy	42.93194	10.52417	40	urban background	8228	NO_2, benzene
Gela - Biviere	it2206a	Italy	37.02249	14.34497	0	rural background	8277	NO_2, O_3, SO_2
Bar2	me0008a	Montenegro	42.10035	19.10348	12	urban background	7721	CO, NO, NO_2, NO_x, O_3, SO_2
Niskic2	me0009a	Montenegro	42.78121	18.94291	629	urban background	7693	CO, NO, NO_2, NO_x, O_3, SO_2
Koper	si0038a	Slovenia	45.54297	13.71354	56	urban background	8198	NO_2, NO_x, O_3
Balikesir-Bandirma	tr100241	Turkey	40.34795	27.97496	38	urban background	8509	NO_2
Canakkale-Lapseki	tr170313	Turkey	40.40307	26.77063	12	rural background	8170	NO_2, NO_x, O_3, $PM_{2.5}$, SO_2
Istanbul-Esenyurt	tr340241	Turkey	41.02028	28.66955	36	urban background	7915	NO_2, NO_x, SO_2
Istanbul-Sultangazi	tr340841	Turkey	41.10197	28.87202	128	urban background	8304	NO_2, NO_x, SO_2

Kirkareli-Luleburgaz-	tr390441	Turkey	41.39841	27.34588	56	rural background	8393	NO_2, SO_2

Appendix C: Example time series for NO_2

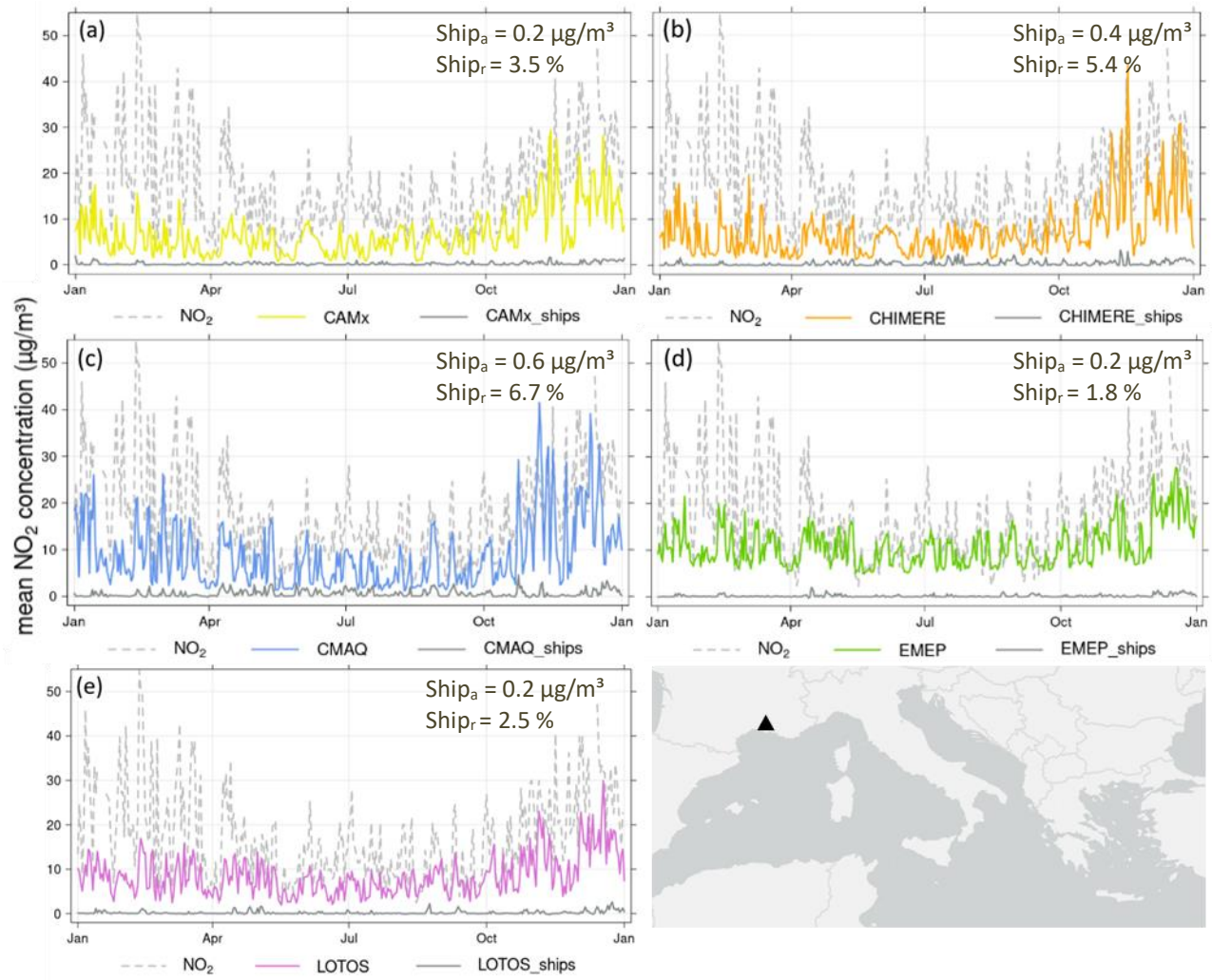

FigureC1: Time series with daily mean NO_2 concentrations in 2015 at station fr08614 in France. The black triangle on the map (bottom right) displays the location of the station. (a) = CAMx, (b) = CHIMERE, (c) = CMAQ, (d) = EMEP, (e) = LOTOS-EUROS. Dashed grey line = measured data, colored lines = modelled data, grey line = modelled potential ship impact. Correlation between modelled and measured data for hourly total emission data for 2015: CAMx = 0.23, CHIMERE = 0.20, CMAQ = 0.60, EMEP = 0.02, LOTOS-EUROS = 0.65. Ship$_a$ displays potential absolute ship impact, Ship$_r$ potential relative ship impact of the respective model.

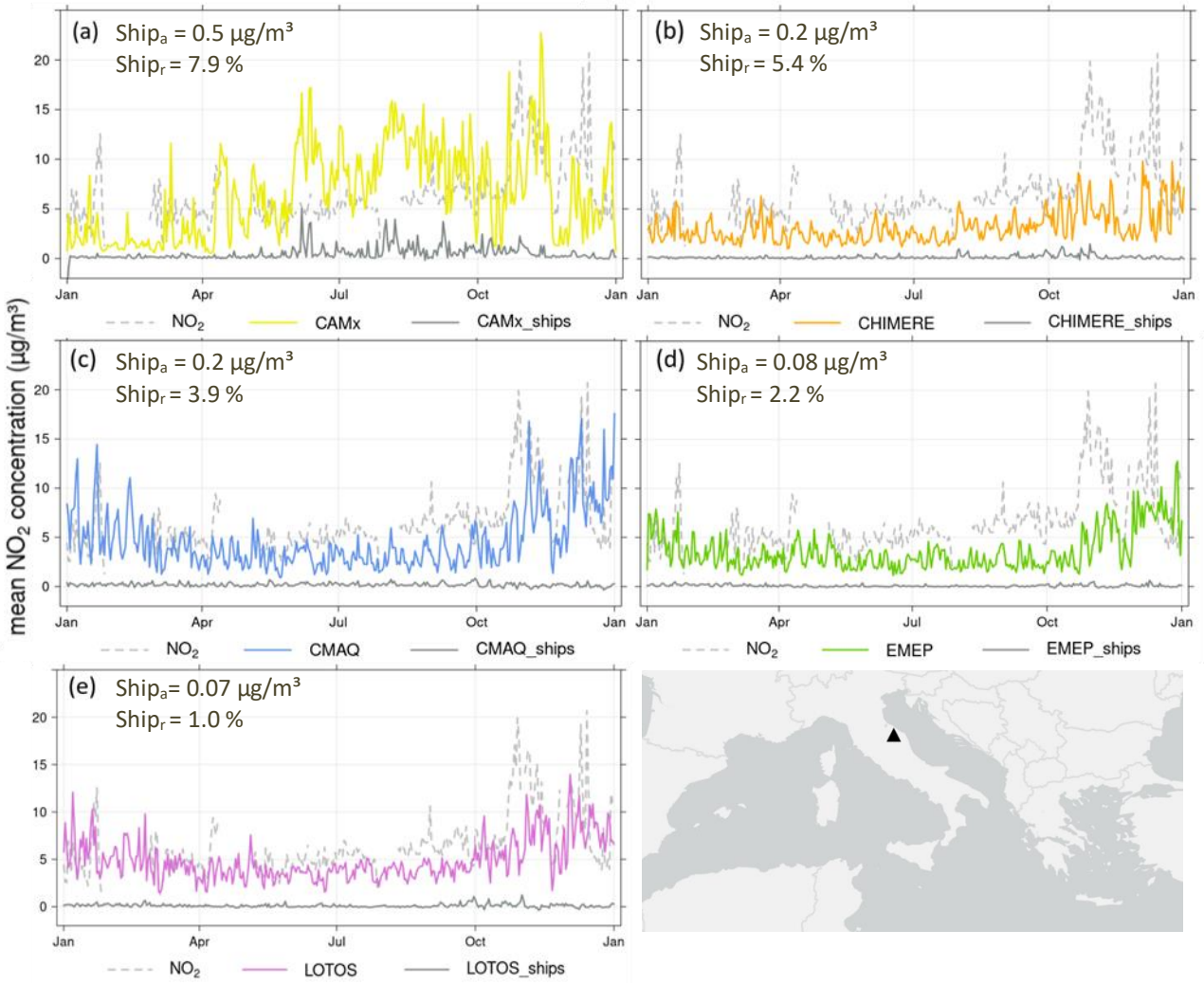

Figure C2: Time series with daily mean NO_2 concentration in 2015 at station it1773a in Italy. The black triangle on the map (bottom right) displays the location of the station. (a) = CAMx, (b) = CHIMERE, (c) = CMAQ, (d) = EMEP, (e) = LOTOS-EUROS. Dashed grey line = measured data, colored lines = modelled data, grey line = modelled ship potential impact. Correlation between modelled and measured data for hourly total emission data for 2015: CAMx = 0.03; CHIMERE = 0.03; CMAQ = 0.20; EMEP = -0.09; LOTOS-EUROS = 0.14 $Ship_a$ displays potential absolute ship impact, $Ship_r$ potential relative ship impact of the respective model.

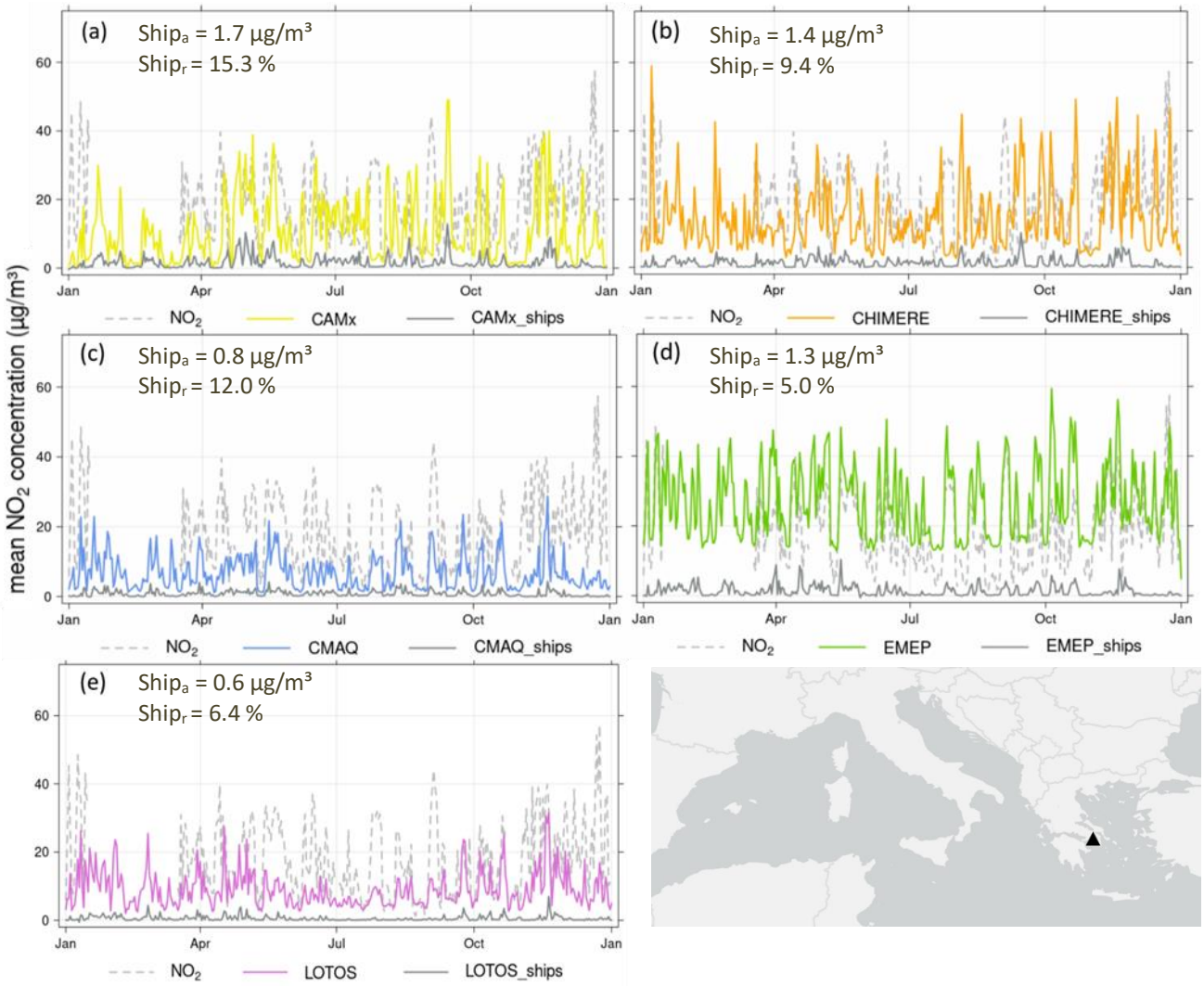

Figure C3: Time series with daily mean NO_2 concentration in 2015 at station gr0035a in Greece. The black triangle on the map (bottom right) displays the location of the station. (a) = CAMx, (b) = CHIMERE, (c) = CMAQ, (d) = EMEP, (e) = LOTOS-EUROS. Dashed grey line = measured data, colored lines = modelled data, grey line = modelled potential ship impact. Correlation between modelled and measured data for hourly total emission data for 2015: CAMx = 0.15; CHIMERE = 0.20; CMAQ = 0.28; EMEP = 0.55; LOTOS-EUROS = 0.38. Ship$_a$ displays potential absolute ship pimpact, Ship$_r$ potential relative ship impact of the respective model.

1105

Appendix D: Example time series for O_3

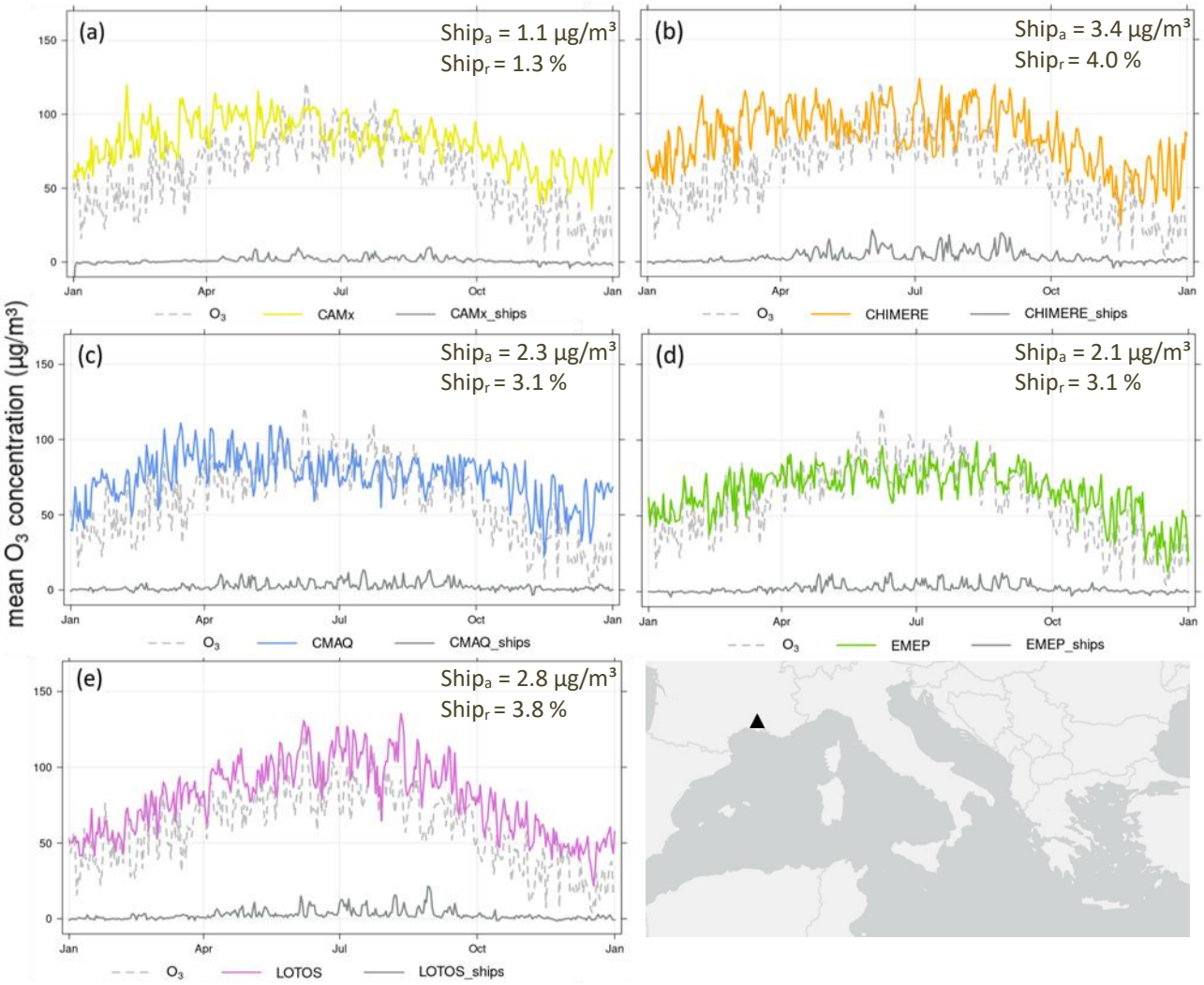

Figure D1: Time series with daily mean O_3 concentration in 2015 at station fr08614 in France. The black triangle on the map (bottom right) displays the location of the station. (a) = CAMx, (b) = CHIMERE, (c) = CMAQ, (d) = EMEP, (e) = LOTOS-EUROS. Dashed gray line = measured data, colored lines = modeled data, gray line = modeled potential ship impact. Correlation between modeled and measured data for hourly total emission data for 2015: CAMx= 0.57; CHIMERE = 0.6; CMAQ = 0.71; EMEP = 0.39; LOTOS-EUROS = 0.78. Ship$_a$ displays potential absolute ship impact, Ship$_r$ potential relative ship impact of the respective model.

1110

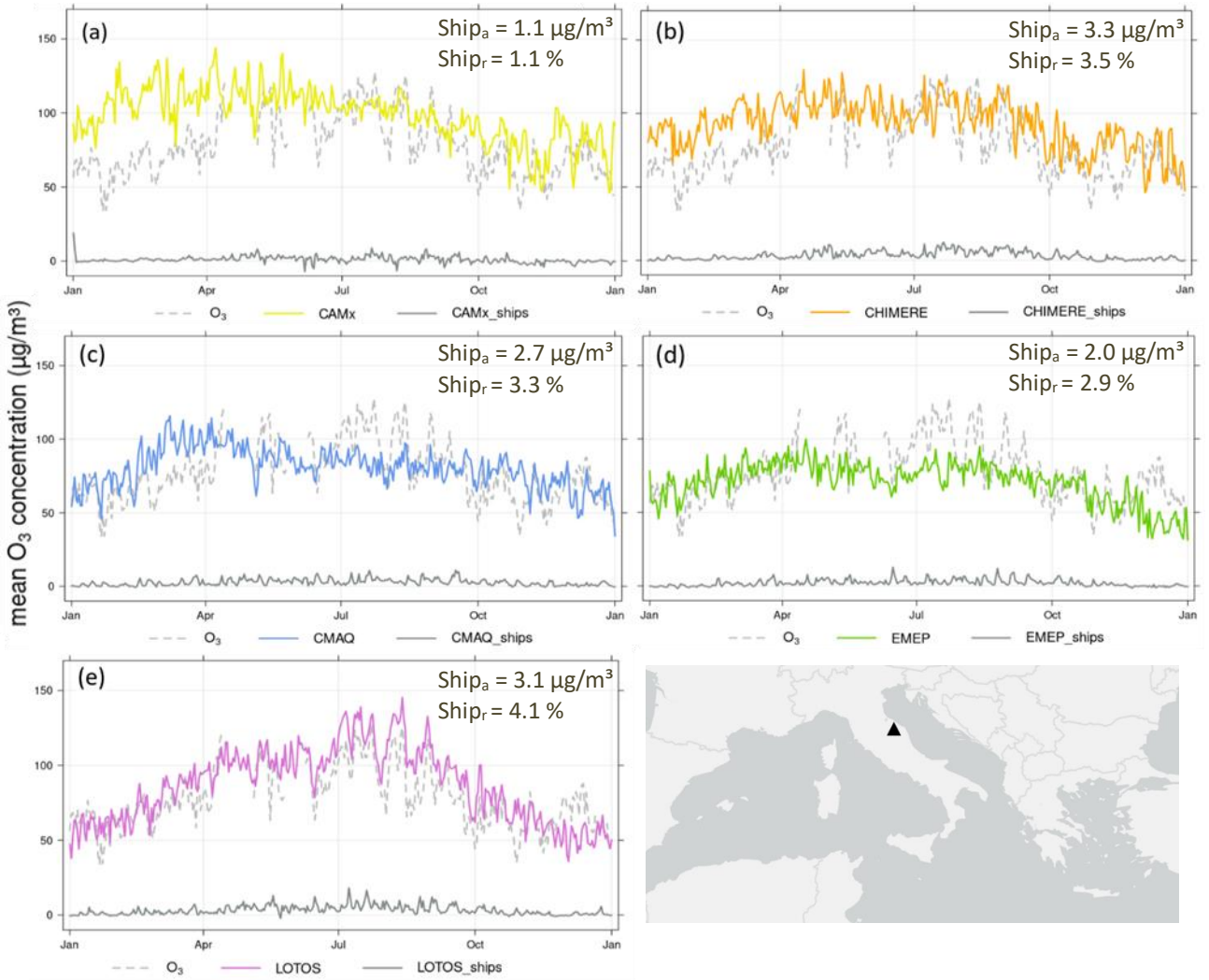

Figure D2: Time series with daily mean O_3 concentration in 2015 at station it1773a in Italy. The black triangle on the map (bottom right) displays the location of the station. (a) = CAMx, (b) = CHIMERE, (c) = CMAQ, (d) = EMEP, (e) = LOTOS-EUROS. Dashed gray line = measured data, colored lines = modeled data, gray line = modeled potential ship impact. Correlation between modeled and measured data for hourly total emission data for 2015: CAMx = 0.37; CHIMERE = 0.4; CMAQ = 0.58; EMEP = 0.35; LOTOS-EUROS = 0.7. $Ship_a$ displays potential absolute ship impact, $Ship_r$ potential relative ship impact of the respective model.

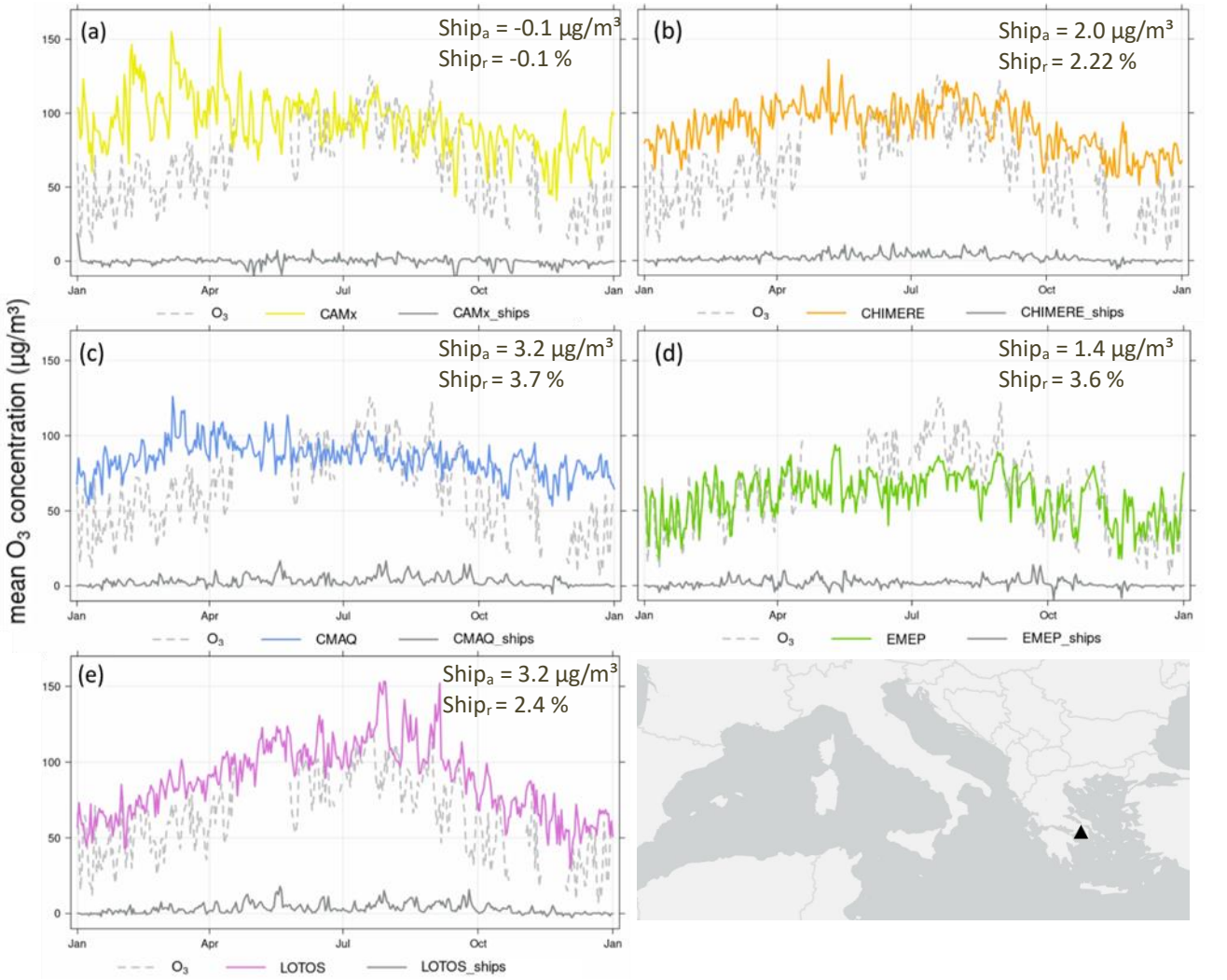

Figure D3: Time series with daily mean O_3 concentration in 2015 at station gr0035a in Greece. The black triangle on the map (bottom right) displays the location of the station. (a) = CAMx, (b) = CHIMERE, (c) = CMAQ, (d) = EMEP, (e) = LOTOS-EUROS. Dashed gray line = measured data, colored lines = modeled data, gray line = modeled potential ship impact. Correlation between modeled and measured data for hourly total emission data for 2015: CAMx = 0.29; CHIMERE = 0.46; CMAQ = 0.50; EMEP = 0.71; LOTOS-EUROS = 0.57. $Ship_a$ displays potential absolute ship impact, $Ship_r$ potential relative ship impact of the respective model.

Appendix E: NO_x Spatial Distribution

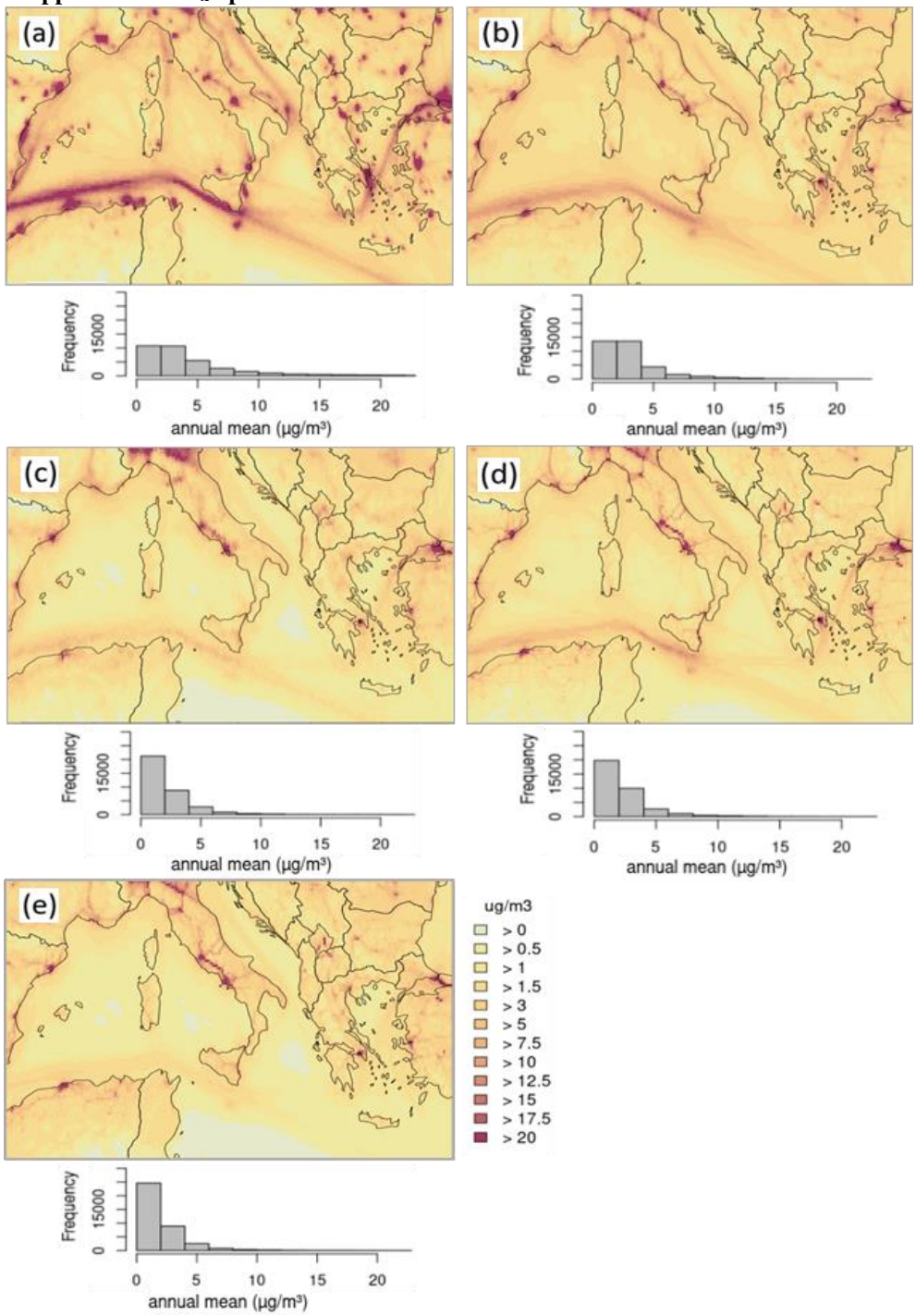

Figure E1: Annual mean of NO_x total concentration. (a) = CAMx, (b) = CHIMERE, (c) = CMAQ, (d) = LOTOS-EUROS. Below the domain figure the respective frequency distribution is displayed for the annual mean NO_x concentration, referred to the whole model domain.

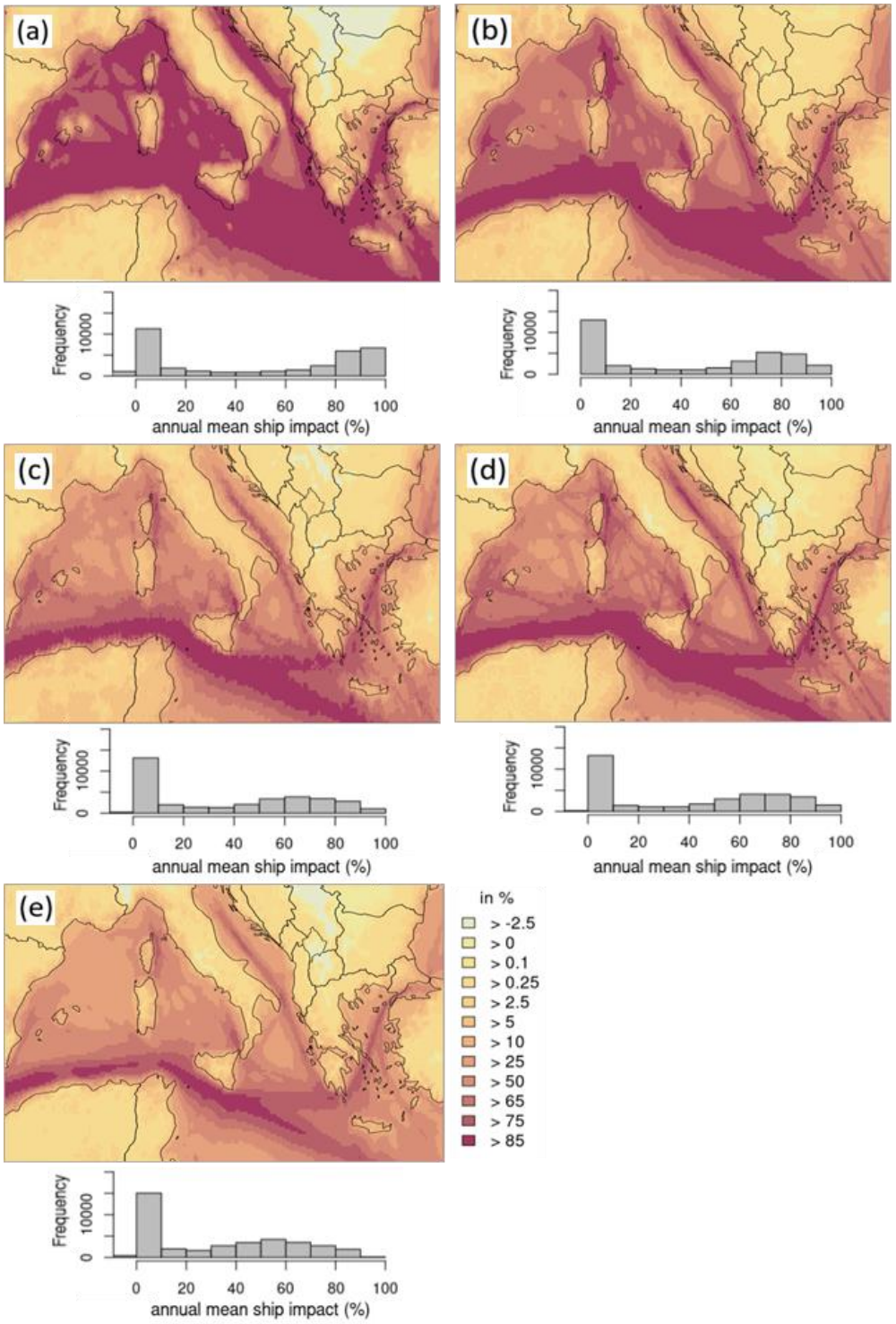

Figure E2: Annual mean relative potential ship impact of NO_x. (a) = CAMx, (b) = CHIMERE, (c) = CMAQ, (d) = LOTOS-EUROS. Below the domain figurethe respective frequency distribution is displayed for the annual mean relative potential ship impact of NO_x, referred to the whole model domain.

1115

Appendix F: annual total dry deposition of N

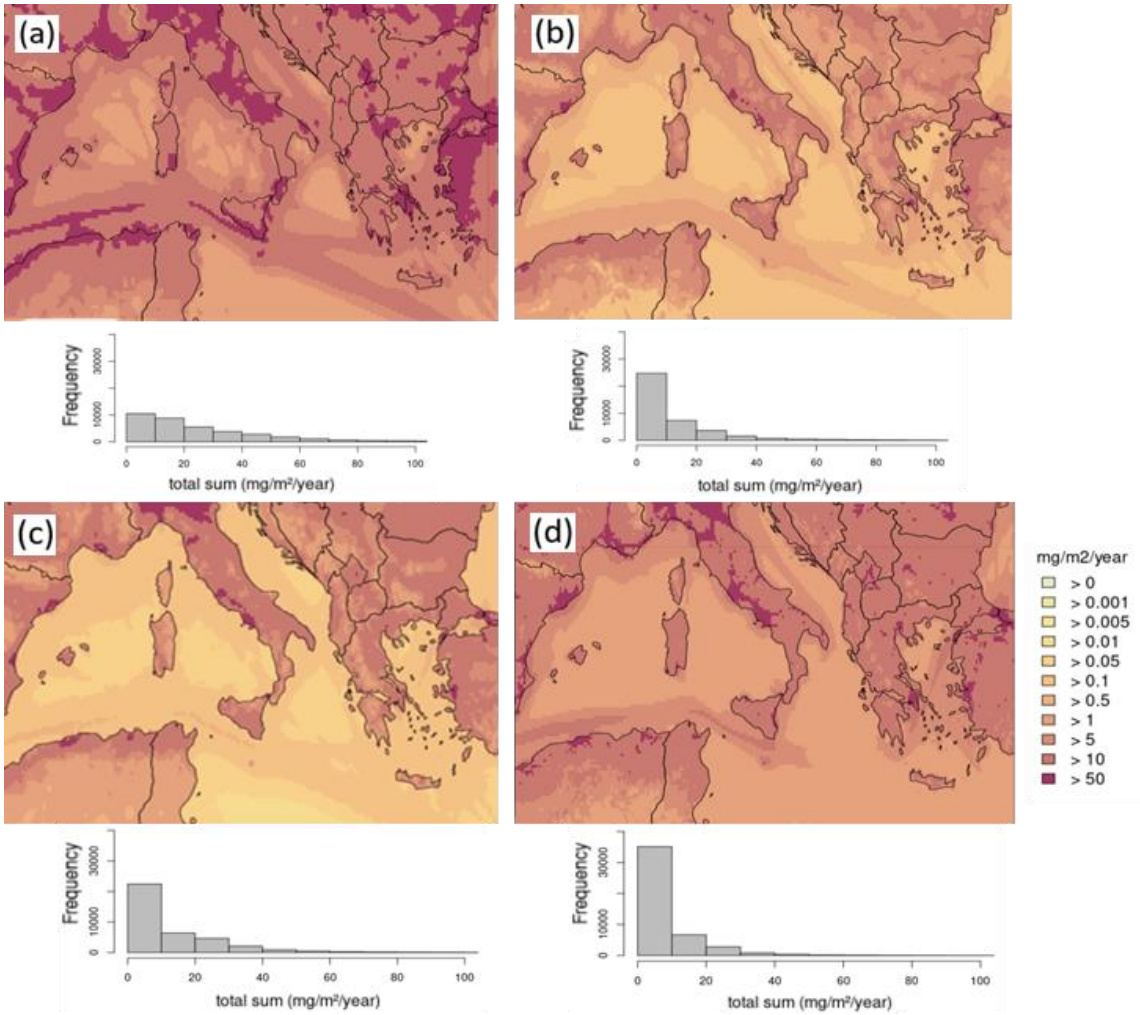

Figure F1: Annual total dry deposition of N. (a) = CAMx, (b) = CHIMERE, (c) = CMAQ, (d) = LOTOS-EUROS.